JOURNAL OF SPACECRAFT AND ROCKETS
Vol. 44, No. 4, July–August 2007

Improved Corrections Process for Constrained Trajectory Design in the *n*-Body Problem

Belinda G. Marchand* and Kathleen C. Howell†
Purdue University, West Lafayette, Indiana 47907-1282
and
Roby S. Wilson‡
Jet Propulsion Laboratory, California Institute of Technology, Pasadena, California 91109

DOI: 10.2514/1.27205

The general objective is the development of efficient techniques for preliminary design of trajectory arcs in nonlinear autonomous dynamic systems in which the desired solution is subject to algebraic interior and/or exterior constraints. For application to the *n*-body problem, trajectories must satisfy specific requirements, e.g., periodicity in terms of the states, interior or boundary constraints, and specified coverage. Thus, a strategy is formulated in a sequence of increasingly complex steps: 1) a trajectory is first modeled as a series of arcs (analytical or numerical) and general trajectory characteristics and timing requirements are established; 2) the specific constraints and associated partials are formulated; 3) a corrections process ensures position and velocity continuity while satisfying the constraints; and finally, 4) the solution is transitioned to a full model employing ephemerides. Though the examples pertain to spacecraft mission design, the methodology is generally applicable to autonomous systems subject to algebraic constraints. For spacecraft mission design applications, an immediate advantage of this approach, particularly for the identification of periodic orbits, is that the startup solution need not exhibit any symmetry to achieve the objectives.

Nomenclature

$A_{k,k-1}, B_{k,k-1}, C_{k,k-1}, D_{k,k-1}$	=	3×3 submatrices of $\Phi(t_k, t_{k-1})$
$A(t)$	=	Jacobian matrix
$\boldsymbol{a}(t) = [\ddot{x}, \ddot{y}, \ddot{z}]^T$	=	column vector that denotes the spacecraft acceleration, km/s^2
$\boldsymbol{f}(\boldsymbol{X})$	=	a nonlinear vector function that depends explicitly on the spacecraft state
N	=	number of patch states along a startup solution
$\boldsymbol{R}(t) = [x, y, z]^T$	=	column vector that denotes spacecraft position, km
t	=	time, s
$\boldsymbol{V}(t) = [\dot{x}, \dot{y}, \dot{z}]^T$	=	column vector that denotes spacecraft velocity, km/s
$\boldsymbol{X}(t) = [\boldsymbol{R}(t), \boldsymbol{V}(t)]^T$	=	column vector that denotes the spacecraft state
x, y, z	=	spacecraft position elements associated with current working reference frame, km
$\dot{x}, \dot{y}, \dot{z}$	=	spacecraft velocity elements associated with current working reference frame, km/s
$\boldsymbol{\alpha}_k$	=	vector of constraints at the kth patch state
α_{kj}	=	the jth element of $\boldsymbol{\alpha}_k$
$\Delta \boldsymbol{V}_k$	=	velocity discontinuity at the kth patch state, km/s
δ	=	prefix denotes a variation measured relative to a reference arc
$\Phi(t_k, t_{k-1})$	=	6×6 state transition matrix from an initial time t_{k-1} to a terminal time t_k

Subscripts

k	=	subscript indicates the quantity is associated with the kth patch state

Superscripts

T	=	superscript denotes transpose operation
$*$	=	superscript indicates the quantity is evaluated along the reference solution

Introduction

FROM a dynamic perspective, the libration points have been the focus of many investigations since the initial work of Poincaré [1]. In the last 20 years, periodic orbits in the three-body regime have successfully served as the basis for trajectory design in various missions [2–8], from the International Sun-Earth Explorer 3 (ISEE-3) [2,3] to the more recent Genesis mission [8]. As the spacecraft applications of multibody orbital analysis continue to expand, the goals and requirements are also becoming evermore challenging. Thus, strategies to isolate preliminary trajectory arcs that satisfy a set of constraints in this regime must be available.

Most optimization schemes, or other analysis tools in the full model, require a good initial guess or startup solution. Thus, the goal of this study is the development of a strategy to more efficiently produce preliminary designs for trajectories, in multibody regimes, when constraints are incorporated. Though the examples presented are related to spacecraft mission design in the *n*-body problem, the generality of the method is preserved to accommodate other applications. Ultimately, this approach represents a feasible numerical scheme for the determination of trajectory arcs in nonlinear autonomous dynamic systems where the desired solution is subject to algebraic interior and/or exterior constraints.

Received 10 August 2006; accepted for publication 17 January 2007.

*Visiting Assistant Professor, School of Aeronautics and Astronautics, Purdue University; currently Assistant Professor, Aerospace Engineering and Engineering Mechanics Department, University of Texas at Austin.

†Hsu Lo Professor of Aeronautical and Astronautical Engineering, School of Aeronautics and Astronautics, Purdue University.

‡Senior Engineer, Guidance Navigation and Control Section, Jet Propulsion Laboratory.

The approach proposed here involves a sequence of increasingly complex steps [9,10]. Initially, the trajectory is modeled as a series of arcs. The arcs may be determined from a three-body model, a multibody numerical solution, or a conic. An arc can also incorporate some additional force, if appropriate, such as solar radiation pressure. This initial analysis is useful in establishing the general trajectory characteristics such as size, orientation, excursions in the in-plane and out-of-plane directions, proximity to specified regions of space (perhaps the libration points), and timing requirements. In the next step in the process, the specific constraints are modeled, as well as the associated partials, if not already available. Then, a differential corrections process is employed to ensure position and velocity continuity along the path while satisfying the constraints. The process can also be used to determine preliminary requirements for maneuvers that may be necessary to satisfy the constraints. In the final step, the trajectory solution is transitioned to a full model that incorporates any desired gravitational bodies, with ephemerides used for the planetary locations. It may include other forces, such as solar radiation pressure, as modeled previously. The focus of this effort, then, is the further development of the mathematical relationships and partials that are necessary to successfully merge the arcs in the three- or n-body environment such that the constraints are satisfied.

Background

In generating a preliminary solution, the capacity to develop a trajectory arc in the three- or four-body problem, one that satisfies a set of constraints, is considered critical for an expanded design tool. For instance, a halo orbit [11] is periodic and symmetric across a fundamental plane in the rotating frame of the restricted problem. Symmetry and periodicity are both, in this case, constrained. However, an orbit can be periodic without being symmetric [12], as is often the case in relative spacecraft motions [13] (i.e., formation flight) near the libration points.

In the restricted three-body problem, where the equations of motion are traditionally formulated in a synodic coordinate system, a typical approach to determine a periodic path is to exploit the symmetry of the mathematical model. First, a startup arc, such as that obtained from the Richardson approximation [14,15], is necessary. Once the startup solution is available, the symmetry properties of the model and the solution of interest, are employed in the design of the differential corrector [11]. However, a differential corrector specifically developed around some geometrical features will naturally only be applicable to trajectories that share those features. A traditional halo corrector, for example, is only useful when searching for trajectories that are simply symmetric about the x–z plane.

As detailed in this investigation, it is possible to specify periodicity as a constraint, without prior knowledge of the symmetry of the solution. Using periodicity as a constraint is particularly useful in exploring periodic orbits near the triangular points, or establishing periodic formations near the libration points. In general, trajectory arcs of any kind can be subject to a wide variety of point constraints during the mission design process. The development is generalized and applicable to any type of point constraint. It is assumed, of course, that the initial guess is still in the vicinity of the desired solution.

Dynamic Model

The elements of the spacecraft state vector $\boldsymbol{X}(t) = [x(t), y(t), z(t), \dot{x}(t), \dot{y}(t), \dot{z}(t)]^T$ represent components of the spacecraft position and velocity, associated with a generic reference frame. Based on this definition, the nonlinear differential equations that govern the evolution of $\boldsymbol{X}(t)$, in any gravitational regime, may be generally represented as

$$\dot{\boldsymbol{X}}(t) = \boldsymbol{f}[\boldsymbol{X}(t)] \tag{1}$$

Let $\boldsymbol{X}^*(t)$ and $\dot{\boldsymbol{X}}^*(t)$ identify a reference state, and the associated time derivative. Then, according to Eq. (1), $\dot{\boldsymbol{X}}^*(t) = \boldsymbol{f}[\boldsymbol{X}^*(t)]$. The general nonlinear state of the spacecraft can always be represented relative to this reference state as follows:

$$\boldsymbol{X}(t) = \boldsymbol{X}^*(t) + \delta\boldsymbol{X}(t) \tag{2}$$

From the definition in Eq. (2), the variational equation associated with Eq. (1) is of the form

$$\delta\dot{\boldsymbol{X}}(t) = A(t)\delta\boldsymbol{X}(t) \tag{3}$$

where

$$A(t) = \left.\frac{\partial \boldsymbol{f}}{\partial \boldsymbol{X}}\right|_{\boldsymbol{X}^*(t)} \tag{4}$$

represents the Jacobian matrix evaluated along the reference solution. The solution to this variational equation is well known and depends on the state transition matrix (STM) $\Phi(t, t_0)$:

$$\delta\boldsymbol{X}(t) = \Phi(t, t_0)\delta\boldsymbol{X}(t_0) \tag{5}$$

The STM is determined by numerical integration of the matrix differential equation

$$\dot{\Phi}(t, t_0) = A(t)\Phi(t, t_0) \tag{6}$$

subject to the initial condition $\Phi(t_0, t_0) = I$, where I denotes a properly dimensioned identity matrix. The variation in Eq. (5) is generally said to be contemporaneous. That is, the variation $\delta\boldsymbol{X}(t)$ is the difference between the actual nonlinear state $\boldsymbol{X}(t)$ and the neighboring nominal state $\boldsymbol{X}^*(t)$, evaluated precisely at time t. However, the derivation of a differential corrections process benefits from the introduction of a noncontemporaneous variation,

$$\delta\boldsymbol{X}' = \delta\bar{X}(t') = \delta\boldsymbol{X}(t) + \dot{\boldsymbol{X}}(t)\delta t \tag{7}$$

where $\delta t = t' - t$ and $\dot{\boldsymbol{X}}$ is evaluated along the current (i.e., the reference) solution. The relation between the contemporaneous and noncontemporaneous variation is illustrated graphically in Fig. 1.

Substitution of Eq. (7) into Eq. (5) yields the following expression:

$$[\delta\boldsymbol{X}_1' - \dot{\boldsymbol{X}}(t_1)\delta t_1] = \Phi(t_1, t_0)[\delta\boldsymbol{X}_0' - \dot{\boldsymbol{X}}(t_0)\delta t_0] \tag{8}$$

If the initial time for the numerical propagation is held fixed, relative to the nominal initial time, then $\delta t_0 = 0$ and Eq. (8) can be further reduced, i.e.,

$$\delta\boldsymbol{X}_1' = \Phi(t_1, t_0)\delta\boldsymbol{X}_0' + \dot{\boldsymbol{X}}_1\delta t_1 \tag{9}$$

Equation (9) is the basis of a standard two-level differential corrector.

Startup Arcs and Patch States

A differential corrections process requires a startup solution. Such a trajectory arc may be the result of a numerical integration process [16], perhaps one such that the path does not necessarily satisfy the specified constraints. An initial guess can also be constructed from a series expansion [14,15] that approximates the solution.

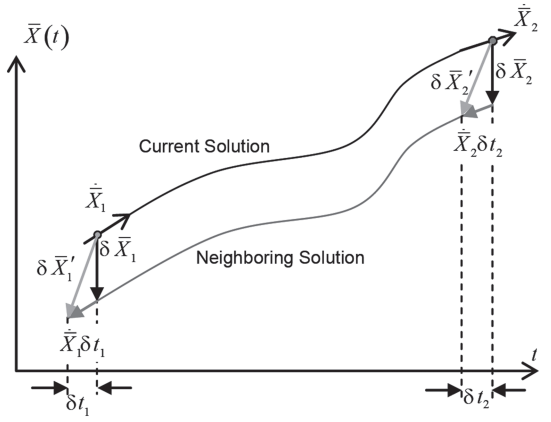

Fig. 1 Contemporaneous vs noncontemporaneous variations.

Other alternatives, even conics, can also serve as a startup arc in the ephemeris model. Once available, the startup solution is decomposed into segments and nodes, or patch points. The process of selecting patch points is somewhat open-ended. It is important, however, that the patch points that are selected adequately capture the overall character and geometry of the solution to ensure convergence. At the same time, too many patch points can unnecessarily constrain the search process and limit the solution space that the corrector is able to identify. For instance, a Lissajous trajectory in the n-body problem is geometrically well behaved. However, due to the dynamically sensitive nature of the region near the libration points, it is best to select at least four patch points per revolution. Although two patch points may be sufficient to converge on a Lissajous trajectory, four will ensure that the overall dimensions of the startup arc are preserved if at all possible. These four patch points may be placed, for instance, at each of the maximum excursion points along the y and z directions in the synodic rotating frame.

Level 1 Differential Corrector

Once a startup arc is identified, the associated patch points are employed in a level 1 corrections process. The goal of the level 1 corrector is simple, that is, to achieve position continuity (in the nonlinear model) across all trajectory segments. The development of the level 1 corrections process [17] is presented here for notational completeness.

Suppose a startup trajectory arc is decomposed into $N-1$ segments and N nodes. Each segment is characterized by an initial time t_{k-1} and a terminal time t_k, where $k = 1, \ldots, N$. At the initial point along a segment, the six-dimensional state vector is defined in terms of two three-element vectors, i.e., $\boldsymbol{X}_{k-1} = [\,\boldsymbol{R}_{k-1} \quad \boldsymbol{V}_{k-1}\,]^T$, whereas the terminal state vector is written $\boldsymbol{X}_k = [\,\boldsymbol{R}_k \quad \boldsymbol{V}_k\,]^T$. The formulation for the level 1 corrector can summarized as follows:

fixed constraints

$$\delta \boldsymbol{R}'_{k-1} = \boldsymbol{0} = \delta \boldsymbol{R}_{k-1}; \qquad \delta t_{k-1} = \delta t_k = 0 \tag{10}$$

targets

$$\delta \boldsymbol{R}'_k = \boldsymbol{R}^*_k - \boldsymbol{R}_k = \delta \boldsymbol{R}_k \tag{11}$$

controls

$$\delta \boldsymbol{V}'_{k-1} = \delta \boldsymbol{V}_{k-1} \tag{12}$$

free

$$\delta \boldsymbol{V}'_k = \delta \boldsymbol{V}_k \tag{13}$$

In essence, a simple targeting scheme (i.e., an automated multiple shooting method) is applied to determine the minimum impulsive maneuver $\Delta \boldsymbol{V}_{k-1}$ necessary to achieve a prespecified terminal position $\boldsymbol{R}_k$. Such a strategy is the basis of a level 1 differential corrector, as illustrated in Fig. 2.

For a multisegment trajectory, the level 1 corrector is sequential; thus, for $k = 1, \ldots, N$, the vector $[\,\boldsymbol{R}^*_{k-1} \quad \boldsymbol{V}^*_{k-1}\,]$ is numerically integrated from t^*_{k-1} to t^*_k. The results of this propagation are represented by the state vector $[\,\boldsymbol{R}_k \quad \boldsymbol{V}_k\,]$. In general, if $\boldsymbol{R}^*_k$ represents the "nominal" position for the terminal node, as specified by the startup arc, and $\boldsymbol{R}_k$ is the actual numerically integrated terminal position vector, then $\delta \boldsymbol{R}'_k = \boldsymbol{R}^*_k - \boldsymbol{R}_k$ denotes the noncontemporaneous position variation. Implementation of the assumptions in Eqs. (10–13), to the illustration in Fig. 1, further implies that $\delta \boldsymbol{R}'_k = \delta \boldsymbol{R}_k$. The control variable that drives the iterative process is $\Delta \boldsymbol{V}_{k-1} = \boldsymbol{V}_{k-1} - \boldsymbol{V}^*_{k-1}$, where $\boldsymbol{V}_{k-1} = \boldsymbol{V}^*_{k-1} + \delta \boldsymbol{V}_{k-1}$; thus, $\Delta \boldsymbol{V}_{k-1} = \delta \boldsymbol{V}_{k-1}$.

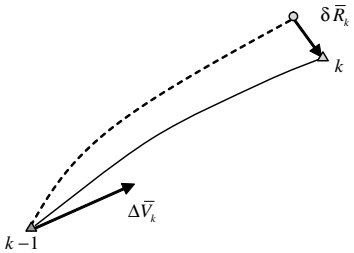

Fig. 2 Stylized representation of the structure for the level 1 differential corrector.

Consider Eq. (8) within the context of the notation in Fig. 2 where, as presently written, $k = 1$. In general, the 6×6 STM, $\Phi(t_k, t_{k-1})$, can be subdivided into four 3×3 submatrices such that

$$\Phi(t_k, t_{k-1}) = \begin{bmatrix} A_{k,k-1} & B_{k,k-1} \\ C_{k,k-1} & D_{k,k-1} \end{bmatrix} \tag{14}$$

The subscript pair "$k, \; k-1$" denotes the direction of the propagation. For example, the right subscript, $k-1$, denotes the start time (t_{k-1}) of the propagation, whereas the subscript to the left, k, reflects the terminal time t_k. Consequently, $\Phi(t_k, t_{k-1})^{-1} = \Phi(t_{k-1}, t_k)$ may also be decomposed into submatrices:

$$\Phi(t_{k-1}, t_k) = \begin{bmatrix} A_{k-1,k} & B_{k-1,k} \\ C_{k-1,k} & D_{k-1,k} \end{bmatrix} \tag{15}$$

Employing this subscript notation in Eq. (8), the variational equations for the segment in Fig. 2 may be rewritten as

$$\begin{bmatrix} \delta \boldsymbol{R}'_k - \boldsymbol{V}_k \delta t_k \\ \delta \boldsymbol{V}'_k - \boldsymbol{a}_k \delta t_k \end{bmatrix} = \begin{bmatrix} A_{k,k-1} & B_{k,k-1} \\ C_{k,k-1} & D_{k,k-1} \end{bmatrix} \begin{bmatrix} \delta \boldsymbol{R}'_{k-1} - \boldsymbol{V}_{k-1} \delta t_{k-1} \\ \delta \boldsymbol{V}'_{k-1} - \boldsymbol{a}_{k-1} \delta t_{k-1} \end{bmatrix} \tag{16}$$

In Eq. (16), $\boldsymbol{V}_k$ and $\boldsymbol{a}_k$ represent the actual nonlinear velocity and acceleration vectors, along the current solution, as highlighted in Fig. 1, at the terminal node. Similarly, $\boldsymbol{V}_{k-1}$ and $\boldsymbol{a}_{k-1}$ are the velocity and acceleration associated with the initial node on the current trajectory segment.

The vector $\delta \boldsymbol{R}'_{k-1}$ is the difference, or noncontemporaneous variation, in position between the initial node on the current solution and the initial node on the nominal solution, as detailed in Fig. 1. The vector $\delta \boldsymbol{V}'_{k-1}$ denotes the noncontemporaneous variation in velocity between the current and nominal solutions. Similar definitions apply for $\delta \boldsymbol{R}'_k$ and $\delta \boldsymbol{V}'_k$.

Note that, in linear systems analysis, the submatrices $A_{k,k-1}$, $B_{k,k-1}$, $C_{k,k-1}$, and $D_{k,k-1}$ are typically associated with a prespecified reference solution, one that is known as a function of time. In a differential corrections process, however, the complete nominal trajectory is not necessarily known a priori. Instead, design constraints are imposed and the goal is to identify an arc that best satisfies these constraints. In this approach, the STM is evaluated along the startup trajectory. The STM, and by implication its submatrices, is subsequently updated during each iteration as the startup arc is modified by the corrections process.

A relationship between the targets and the control variables is obtained from direct application of Eqs. (13–15) to the variational Eq. (16), that is,

$$\delta \boldsymbol{V}_{k-1} = B^{-1}_{k,k-1} \left(\boldsymbol{R}^*_k - \boldsymbol{R}_k \right) \tag{17}$$

If this change in initial velocity $\delta \boldsymbol{V}_{k-1}$ is applied to the current initial velocity $\boldsymbol{V}_{k-1}$, the error in final position $\boldsymbol{R}^*_k - \boldsymbol{R}_k$ should become smaller with each successive iteration. Note that a similar relationship can be derived by applying the constraints in Eq. (10) to the inverse of Eq. (16). This eventually reveals that

$$B_{k,k-1} = \left(C_{k-1,k} - D_{k-1,k} B^{-1}_{k-1,k} A_{k-1,k} \right)^{-1} \tag{18}$$

where the submatrices with subscript $k, \; k-1$ are associated with $\Phi(t_k, t_{k-1})$, whereas those with subscript $k-1, k$ are the submatrices corresponding to $\Phi(t_{k-1}, t_k) = \Phi(t_k, t_{k-1})^{-1}$.

Level 2 Differential Corrector

In a study by Wilson and Howell [10], the initial development of the two-level constrained corrector is presented. In particular, the two-level corrector developed by Howell and Pernicka [17] is

augmented with terminal boundary constraints on radial distance, time, inclination, apse condition, and state.

The process is applied to the initial design of the Genesis trajectory. In the present investigation, a generalization of this methodology is developed and implemented as an end-to-end mission design tool.

The level 2 differential corrector is a procedure based on three or more patch points. The goal of the level 2 corrector is to simultaneously determine a set of adjustments, or modifications, in the state elements for all of the nodes (or patch points) to meet some given set of constraints. Of the N nodes available, the first and last are termed the initial and final states. All the remaining nodes are termed interior patch points. Hence, if there are N patch points, then $N-2$ of these nodes are interior patch points.

An example problem with three patch points is represented in Fig. 3, where the subscript $k-1$ denotes the initial state along one segment, $k+1$ identifies the final state on the next segment, and k is associated with the interior state that connects the two consecutive segments. The state vector at the initiation of a numerical propagation process is labeled with a $+$ superscript, whereas that at the end of a propagation is labeled with the $-$ superscript. The goal of the level 1 corrections process is to achieve position continuity across segments $\boldsymbol{R}_k^+ = \boldsymbol{R}_k^-$. Once position continuity is achieved, the next level of the corrections process enforces any given number of constraints on any of the N patch points available. For instance, Howell and Pernicka [17] employ a two-level corrector to enforce velocity continuity at each of the interior points. In this case, three scalar constraints are imposed on each interior point, $\boldsymbol{V}_k^+ = \boldsymbol{V}_k^-$ for $k = 2, \ldots, N-1$.

Velocity continuity across segments is formulated as a constraint [10,17], applied at the kth node, such that $\boldsymbol{V}_k^+ - \boldsymbol{V}_k^- - \Delta\boldsymbol{V}_k^* = \boldsymbol{0}$, where $\Delta\boldsymbol{V}_k^*$ represents the desired value of the impulsive maneuver at the kth node. Then, the goal of a level 2 corrections process is to minimize the constraint error.

The control variables available to enforce the constraints at the nodes are the positions and times associated with the nodes themselves. Thus, the patch points in the level 2 corrector are allowed to "float" in a sense.

The next step in a generalized level 2 corrector is to establish a relationship between the control variables and the constraint equations. To that end, consider the following set of variational equations associated with each of the segments in Fig. 3, i.e.,

$$\begin{bmatrix} (\delta\boldsymbol{R}'_k)^- - \boldsymbol{V}_k^-\delta t_k^- \\ (\delta\boldsymbol{V}'_k)^- - \boldsymbol{a}_k^-\delta t_k^- \end{bmatrix} = \begin{bmatrix} A_{k,k-1} & B_{k,k-1} \\ C_{k,k-1} & D_{k,k-1} \end{bmatrix} \begin{bmatrix} (\delta\boldsymbol{R}'_{k-1})^+ - \boldsymbol{V}_{k-1}^+\delta t_{k-1}^+ \\ (\delta\boldsymbol{V}'_{k-1})^+ - \boldsymbol{a}_{k-1}^+\delta t_{k-1}^+ \end{bmatrix} \tag{19}$$

$$\begin{bmatrix} (\delta\boldsymbol{R}'_k)^+ - \boldsymbol{V}_k^+\delta t_k^+ \\ (\delta\boldsymbol{V}'_k)^+ - \boldsymbol{a}_k^+\delta t_k^+ \end{bmatrix} = \begin{bmatrix} A_{k,k+1} & B_{k,k+1} \\ C_{k,k+1} & D_{k,k+1} \end{bmatrix} \begin{bmatrix} (\delta\boldsymbol{R}'_{k+1})^- - \boldsymbol{V}_{k+1}^-\delta t_{k+1}^- \\ (\delta\boldsymbol{V}'_{k+1})^- - \boldsymbol{a}_{k+1}^-\delta t_{k+1}^- \end{bmatrix} \tag{20}$$

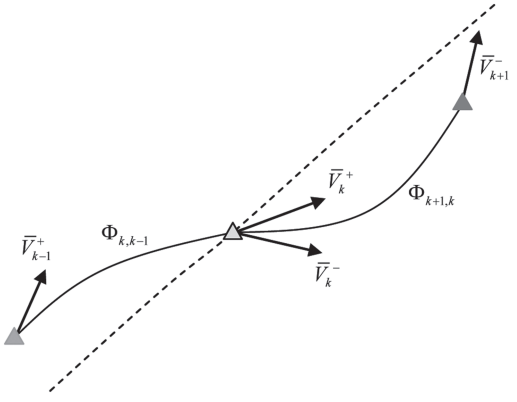

Fig. 3 Stylized representation of level 2 differential corrector.

Note that, in Eq. (20), the flow of the second segment is reversed to evolve from t_{k+1} to t_k. In the present development, each trajectory segment is treated independently with respect to the rest of the segments along the solution. For example, the variations in the initial state at t_{k-1}^+ do not directly affect changes on the second segment, from t_k^+ to t_{k+1}^-. This segment independence results directly from the sequential nature of the level 1 corrector. Using the same terminology employed previously, the formulation for this particular level 2 differential corrector is as follows:

fixed constraints

$$\bar{R}_k^+ - \bar{R}_k^- = \bar{0}; \qquad t_k^+ - t_k^- = 0 \tag{21}$$

targets

$$\left(\bar{V}_k^+ - \bar{V}_k^-\right) - \Delta\bar{V}_k^* = \delta\bar{V}_k^+ - \delta\bar{V}_k^- - \Delta\bar{V}_k^* \tag{22}$$

controls

$$\delta\bar{R}_{k-1}, \delta t_{k-1}, \delta\bar{R}_k, \delta t_k, \delta\bar{R}_{k+1}, \delta t_{k+1} \tag{23}$$

free

$$\delta\bar{V}_{k-1}^+, \delta\bar{V}_{k+1}^- \tag{24}$$

Note that, if a deterministic maneuver is allowed at the kth node, then $\Delta\boldsymbol{V}_k^* \neq \boldsymbol{0}$. Based on Eq. (22), there are $(N-2)\times 3$ targets, three for each interior patch point. The control variables, as previously stated, are the position and times of all N patch points. Thus, in general, there are $N\times 4$ control parameters. Beyond the initial investigation by Howell and Pernicka [17], it is also possible to specify arbitrary constraints at any of the N patch points [10]. These constraints become additional targets in a level 2 corrections process. In the following section, additional constraints are presented to supplement those originally presented by Wilson and Howell [10] and expand the generality of the method. Note that, unless too many constraints are specified, this system will naturally be underdetermined.

To solve the subproblem in Fig. 3, it is necessary to relate the target to the control variables, $\delta\boldsymbol{R}_{k-1}$, δt_{k-1}, $\delta\boldsymbol{R}_k$, δt_k, $\delta\boldsymbol{R}_{k+1}$, and δt_{k+1}. In the case of the velocity continuity constraint, the following approximations are necessary:

$$\delta\boldsymbol{V}_k^- = \left(\frac{\partial\boldsymbol{V}_k^-}{\partial\boldsymbol{R}_{k-1}}\right)\delta\boldsymbol{R}_{k-1} + \left(\frac{\partial\boldsymbol{V}_k^-}{\partial t_{k-1}}\right)\delta t_{k-1} + \left(\frac{\partial\boldsymbol{V}_k^-}{\partial\boldsymbol{R}_k}\right)\delta\boldsymbol{R}_k + \left(\frac{\partial\boldsymbol{V}_k^-}{\partial t_k}\right)\delta t_k \tag{25}$$

$$\delta\boldsymbol{V}_k^+ = \left(\frac{\partial\boldsymbol{V}_k^+}{\partial\boldsymbol{R}_k}\right)\delta\boldsymbol{R}_k + \left(\frac{\partial\boldsymbol{V}_k^+}{\partial t_k}\right)\delta t_k + \left(\frac{\partial\boldsymbol{V}_k^+}{\partial\boldsymbol{R}_{k+1}}\right)\delta\boldsymbol{R}_{k+1} + \left(\frac{\partial\boldsymbol{V}_k^+}{\partial t_{k+1}}\right)\delta t_{k+1} \tag{26}$$

In the level 2 formulation, the partial derivatives are evaluated along the current trajectory. As a result, the variations are defined as $\delta\boldsymbol{V}_k^- = (\boldsymbol{V}_k^-)^* - \boldsymbol{V}_k^-$ and $\delta\boldsymbol{V}_k^+ = (\boldsymbol{V}_k^+)^* - \boldsymbol{V}_k^+$, and the velocity continuity constraint is

$$\delta\boldsymbol{V}_k^+ - \delta\boldsymbol{V}_k^- = \left(\boldsymbol{V}_k^+\right)^* - \left(\boldsymbol{V}_k^-\right)^* - \left(\boldsymbol{V}_k^+ - \boldsymbol{V}_k^-\right) = \Delta\boldsymbol{V}_k^* - \Delta\boldsymbol{V}_k \tag{27}$$

This function can be obtained by subtracting Eq. (26) from Eq. (25):

$$\delta\Delta\boldsymbol{V}_k = \Delta\boldsymbol{V}_k^* - \Delta\boldsymbol{V}_k = \left(-\frac{\partial\boldsymbol{V}_k^-}{\partial\boldsymbol{R}_{k-1}}\right)\delta\boldsymbol{R}_{k-1} + \left(-\frac{\partial\boldsymbol{V}_k^-}{\partial t_{k-1}}\right)\delta t_{k-1} + \left(\frac{\partial\boldsymbol{V}_k^+}{\partial\boldsymbol{R}_k} - \frac{\partial\boldsymbol{V}_k^-}{\partial\boldsymbol{R}_k}\right)\delta\boldsymbol{R}_k + \left(\frac{\partial\boldsymbol{V}_k^+}{\partial t_k} - \frac{\partial\boldsymbol{V}_k^-}{\partial t_k}\right)\delta t_k + \left(\frac{\partial\boldsymbol{V}_k^+}{\partial\boldsymbol{R}_{k+1}}\right)\delta\boldsymbol{R}_{k+1} + \left(\frac{\partial\boldsymbol{V}_k^+}{\partial t_{k+1}}\right)\delta t_{k+1} \tag{28}$$

Table 1 Level 2 partial derivatives of velocity discontinuity across patch states

Partials with respect to position	Partials with respect to time
$\frac{\partial \Delta \boldsymbol{V}_k}{\partial \boldsymbol{R}_{k-1}} = \left(-\frac{\partial \boldsymbol{V}_k^-}{\partial \boldsymbol{R}_{k-1}}\right)$	$\frac{\partial \Delta \boldsymbol{V}_k}{\partial t_{k-1}} = \left(-\frac{\partial \boldsymbol{V}_k^-}{\partial t_{k-1}}\right)$
$\frac{\partial \Delta \boldsymbol{V}_k}{\partial \boldsymbol{R}_k} = \left(\frac{\partial \boldsymbol{V}_k^+}{\partial \boldsymbol{R}_k} - \frac{\partial \boldsymbol{V}_k^-}{\partial \boldsymbol{R}_k}\right)$	$\frac{\partial \Delta \boldsymbol{V}_k}{\partial t_k} = \left(\frac{\partial \boldsymbol{V}_k^+}{\partial t_k} - \frac{\partial \boldsymbol{V}_k^-}{\partial t_k}\right)$
$\frac{\partial \Delta \boldsymbol{V}_k}{\partial \boldsymbol{R}_{k+1}} = \left(\frac{\partial \boldsymbol{V}_k^+}{\partial \boldsymbol{R}_{k+1}}\right)$	$\frac{\partial \Delta \boldsymbol{V}_k}{\partial t_{k+1}} = \left(\frac{\partial \boldsymbol{V}_k^+}{\partial t_{k+1}}\right)$

Equation (28) is basically a Taylor series expansion of $\Delta \boldsymbol{V}_k$; hence, the definitions in Table 1 are immediately apparent.

The determination of each of the partial derivatives in Table 1 is accomplished through a finite difference approach. For example, to isolate the variation of $\boldsymbol{V}_k^-$ with respect to $\boldsymbol{R}_{k-1}$, all other independent control variables are set to zero in the variational equations for the relevant segment

$$\delta \boldsymbol{R}_k = \delta \boldsymbol{R}_{k+1} = \boldsymbol{0} \tag{29}$$

$$\delta t_{k-1} = \delta t_k = \delta t_{k+1} = 0 \tag{30}$$

As a result, the partial derivative can be approximated as $\partial \boldsymbol{V}_k^- / \partial \boldsymbol{R}_{k-1} \approx \delta \boldsymbol{V}_k^- / \delta \boldsymbol{R}_{k-1}$. The variations necessary to construct these partials may be obtained through algebraic manipulation of the variational Eqs. (19) or (20). The results of this finite difference approximation are presented in Table 2.

For the level 2 velocity continuity constraint, substitution of the preceding partials into the expressions in Table 1 leads to the results in Table 3. The traditional statement [17] of the level 2 corrector is

$$\delta \Delta \boldsymbol{V}_k = \Delta \boldsymbol{V}_k^* - \Delta \boldsymbol{V}_k = \underbrace{\begin{bmatrix} \frac{\partial \Delta \boldsymbol{V}_k}{\partial \boldsymbol{R}_{k-1}} & \frac{\partial \Delta \boldsymbol{V}_k}{\partial t_{k-1}} & \frac{\partial \Delta \boldsymbol{V}_k}{\partial \boldsymbol{R}_k} & \frac{\partial \Delta \boldsymbol{V}_k}{\partial t_k} & \frac{\partial \Delta \boldsymbol{V}_k}{\partial \boldsymbol{R}_{k+1}} & \frac{\partial \Delta \boldsymbol{V}_k}{\partial t_{k+1}} \end{bmatrix}}_{M} \underbrace{\begin{bmatrix} \delta \boldsymbol{R}_{k-1} \\ \delta t_{k-1} \\ \delta \boldsymbol{R}_k \\ \delta t_k \\ \delta \boldsymbol{R}_{k+1} \\ \delta t_{k+1} \end{bmatrix}}_{\boldsymbol{b}} \tag{31}$$

In Eq. (31), the matrix M, containing all of the partial derivatives in Table 3, is termed the state relationship matrix (SRM) and $\boldsymbol{b}$ denotes the vector of variations in position and time. The linear system in Eq. (31) can subsequently be summarized as $\delta \Delta \boldsymbol{V}_k = M \boldsymbol{b}$.

Table 2 Partial derivatives of velocity relative to patch state control variables

Partials with respect to position	Partials with respect to time
$\frac{\partial \boldsymbol{V}_k^-}{\partial \boldsymbol{R}_{k-1}} = B_{k-1,k}^{-1}$	$\frac{\partial \boldsymbol{V}_k^-}{\partial t_{k-1}} = -B_{k-1,k}^{-1} \boldsymbol{V}_{k-1}^+$
$\frac{\partial \boldsymbol{V}_k^-}{\partial \boldsymbol{R}_k} = -B_{k-1,k}^{-1} A_{k-1,k}$	$\frac{\partial \boldsymbol{V}_k^-}{\partial t_k} = \left(\boldsymbol{a}_k^- - D_{k,k-1} B_{k,k-1}^{-1} \boldsymbol{V}_k^-\right)$
$\frac{\partial \boldsymbol{V}_k^+}{\partial \boldsymbol{R}_k} = -B_{k+1,k}^{-1} A_{k+1,k}$	$\frac{\partial \boldsymbol{V}_k^+}{\partial t_k} = \left(\boldsymbol{a}_k^+ - D_{k,k+1} B_{k,k+1}^{-1} \boldsymbol{V}_k^+\right)$
$\frac{\partial \boldsymbol{V}_k^+}{\partial \boldsymbol{R}_{k+1}} = B_{k+1,k}^{-1}$	$\frac{\partial \boldsymbol{V}_k^+}{\partial t_{k+1}} = -B_{k+1,k}^{-1} \boldsymbol{V}_{k+1}^-$

In a well-posed problem, the system is underdetermined; that is, there are more control variables than target quantities. Hence, an infinite number of solutions exist. In a traditional corrections process, the minimum Euclidean norm solution is selected. The minimum-norm solution is well known and computed as

$$\boldsymbol{b} = M^T (M M^T)^{-1} \delta \Delta \boldsymbol{V}_k \tag{32}$$

The results from Eq. (32) suggest possible changes in the positions and times of each patch state that may minimize the constraint equations. These changes are applied in the nonlinear system and the level 1 iteration is repeated to achieve position continuity. Of course, the changes suggested by Eq. (32) only lead to a minimum-norm solution in the linear system. In reality, it is unlikely that the modified nonlinear path will exactly satisfy the constraints after position continuity is reestablished in the nonlinear system.

At best, the updated nonlinear path will more closely follow the given constraints. Ultimately, if a solution exists in the nonlinear system, the interior values of $\Delta \boldsymbol{V}_k$ should decrease, or approach the nominal value, with every successive iteration.

Level 2 with Constraints

It is frequently necessary to specify additional constraints along a particular trajectory. The level 2 differential corrector described in the preceding section can be modified to allow general constraints at any of the patch points that describe the solution. Incorporating constraints at any patch point is possible as long as the constraint is of the form

$$\alpha_{kj} = \alpha_{kj}\left(\boldsymbol{R}_k, \boldsymbol{V}_k^+, \boldsymbol{V}_k^-, t_k\right) \tag{33}$$

or

$$\alpha_{kj} = \alpha_{kj}(\boldsymbol{R}_k, \boldsymbol{V}_k, t_k) \tag{34}$$

Thus, the scalar constraint α_{kj} must be expressed as a function of the position, velocity, and time that correspond to the patch point. The first subscript index, k, on the constraint denotes the patch point with which the constraint is associated. The second index j denotes the constraint number at that patch point. This allows for multiple constraints at multiple patch points. Let α_{kj}^* represent the desired value of this algebraic constraint. Recall that the control variables in a level 2 corrector are $\delta \boldsymbol{R}_{k-1}$, δt_{k-1}, $\delta \boldsymbol{R}_k$, δt_k, $\delta \boldsymbol{R}_{k+1}$, and δt_{k+1}. To incorporate these constraints into the corrections process, it is necessary to establish a relationship between the targets, $\delta \alpha_{kj} = \alpha_{kj}^* - \alpha_{kj}$, and the control variables. By definition, α_{kj} can depend explicitly on $\boldsymbol{R}_k$ and t_k. However, there is no explicit dependence on the remaining control variables. Instead, the constraint may also depend on either $\boldsymbol{V}_k^+$ or $\boldsymbol{V}_k^-$, or both. Such a functional form introduces an implicit dependence on the other control variables because the velocity discontinuities at the kth patch point are related to the position and times of the nodes neighboring the patch point of interest; in particular,

$$\boldsymbol{V}_k^+ = \boldsymbol{V}_k^+(\boldsymbol{R}_k, t_k, \boldsymbol{R}_{k+1}, t_{k+1}) \tag{35}$$

$$\boldsymbol{V}_k^- = \boldsymbol{V}_k^-(\boldsymbol{R}_{k-1}, t_{k-1}, \boldsymbol{R}_k, t_k) \tag{36}$$

Thus, the constraint equation can also be approximated, to the first order, through the following Taylor series expansion:

Table 3 Summary of partial derivatives for level 2: velocity constraints at interior patch points

Partials with respect to position	Partials with respect to time
$\frac{\partial \Delta \boldsymbol{V}_k}{\partial \boldsymbol{R}_{k-1}} = -B_{k-1,k}^{-1}$	$\frac{\partial \Delta \boldsymbol{V}_k}{\partial t_{k-1}} = B_{k-1,k}^{-1} \boldsymbol{V}_{k-1}^+$
$\frac{\partial \Delta \boldsymbol{V}_k}{\partial \boldsymbol{R}_k} = B_{k-1,k}^{-1} A_{k-1,k} - B_{k+1,k}^{-1} A_{k+1,k}$	$\frac{\partial \Delta \boldsymbol{V}_k}{\partial t_k} = \boldsymbol{a}_k^+ - \boldsymbol{a}_k^- + D_{k,k-1} B_{k,k-1}^{-1} \boldsymbol{V}_k^- - D_{k,k+1} B_{k,k+1}^{-1} \boldsymbol{V}_k^+$ or $\frac{\partial \Delta \boldsymbol{V}_k}{\partial t_k} = \boldsymbol{a}_k^+ - \boldsymbol{a}_k^- - B_{k-1,k}^{-1} A_{k-1,k} \boldsymbol{V}_k^- + B_{k+1,k}^{-1} A_{k+1,k} \boldsymbol{V}_k^+$
$\frac{\partial \Delta \boldsymbol{V}_k}{\partial \boldsymbol{R}_{k+1}} = B_{k+1,k}^{-1}$	$\frac{\partial \Delta \boldsymbol{V}_k}{\partial t_{k+1}} = -B_{k+1,k}^{-1} \boldsymbol{V}_{k+1}^-$

$$\alpha^*_{kj} = \alpha_{kj} + \left(\frac{\partial \alpha_{kj}}{\delta \boldsymbol{R}_{k-1}} + \frac{\partial \alpha_{kj}}{\partial \bar{V}^+_k}\frac{\partial \boldsymbol{V}^+_k}{\partial \boldsymbol{R}_{k-1}} + \frac{\partial \alpha_{kj}}{\partial \boldsymbol{V}^-_k}\frac{\partial \boldsymbol{V}^-_k}{\partial \boldsymbol{R}_{k-1}}\right)\delta \boldsymbol{R}_{k-1}$$
$$+ \left(\frac{\partial \alpha_{kj}}{\delta t_{k-1}} + \frac{\partial \alpha_{kj}}{\partial \boldsymbol{V}^+_k}\frac{\partial \boldsymbol{V}^+_k}{\partial t_{k-1}} + \frac{\partial \alpha_{kj}}{\partial \boldsymbol{V}^-_k}\frac{\partial \boldsymbol{V}^-_k}{\partial t_{k-1}}\right)\delta t_{k-1}$$
$$+ \left(\frac{\partial \alpha_{kj}}{\partial \bar{R}_k} + \frac{\partial \alpha_{kj}}{\partial \bar{V}^+_k}\frac{\partial \bar{V}^+_k}{\partial \bar{R}_k} + \frac{\partial \alpha_{kj}}{\partial \bar{V}^-_k}\frac{\partial \bar{V}^-_k}{\partial \bar{R}_k}\right)\delta \bar{R}_k$$
$$+ \left(\frac{\partial \alpha_{kj}}{\delta t_k} + \frac{\partial \alpha_{kj}}{\partial \bar{V}^+_k}\frac{\partial \bar{V}^+_k}{\partial t_k} + \frac{\partial \alpha_{kj}}{\partial \bar{V}^-_k}\frac{\partial \bar{V}^-_k}{\partial t_k}\right)\delta t_k$$
$$+ \left(\frac{\partial \alpha_{kj}}{\delta \bar{R}_{k+1}} + \frac{\partial \alpha_{kj}}{\partial \bar{V}^+_k}\frac{\partial \bar{V}^+_k}{\partial \bar{R}_{k+1}} + \frac{\partial \alpha_{kj}}{\partial \bar{V}^-_k}\frac{\partial \bar{V}^-_k}{\partial \bar{R}_{k+1}}\right)\delta \bar{R}_{k+1}$$
$$+ \left(\frac{\partial \alpha_{kj}}{\delta t_{k+1}} + \frac{\partial \alpha_{kj}}{\partial \bar{V}^+_k}\frac{\partial \bar{V}^+_k}{\partial t_{k+1}} + \frac{\partial \alpha_{kj}}{\partial \bar{V}^-_k}\frac{\partial \bar{V}^-_k}{\partial t_{k+1}}\right)\delta t_{k+1} \tag{37}$$

The partial derivatives in Eq. (37) are evaluated along the current solution. This expression may be further simplified by applying the definitions in Eqs. (33), (35), and (36), that is,

$$\frac{\partial \alpha_{kj}}{\partial \boldsymbol{R}_{k-1}} = \frac{\partial \alpha_{kj}}{\partial \boldsymbol{R}_{k+1}} = \boldsymbol{0}^T \tag{38}$$

$$\frac{\partial \alpha_{kj}}{\partial t_{k-1}} = \frac{\partial \alpha_{kj}}{\partial t_{k+1}} = 0 \tag{39}$$

$$\frac{\partial \boldsymbol{V}^+_k}{\partial \boldsymbol{R}_{k-1}} = \frac{\partial \boldsymbol{V}^-_k}{\partial \boldsymbol{R}_{k+1}} = 0_{3\times 3} \tag{40}$$

$$\frac{\partial \boldsymbol{V}^+_k}{\partial t_{k-1}} = \frac{\partial \boldsymbol{V}^-_k}{\partial t_{k+1}} = \boldsymbol{0} \tag{41}$$

In Eqs. (38–41), $\boldsymbol{0}^T$ denotes a 1×3 row vector of zeros and $0_{3\times 3}$ represents the 3×3 zero matrix. Substitution of Eqs. (38–41) into Eq. (37) leads to the following variational constraint equation:

$$\delta \alpha_{kj} = \left(\frac{\partial \alpha_{kj}}{\partial \boldsymbol{V}^-_k}\frac{\partial \boldsymbol{V}^-_k}{\partial \boldsymbol{R}_{k-1}}\right)\delta \boldsymbol{R}_{k-1} + \left(\frac{\partial \alpha_{kj}}{\partial \boldsymbol{V}^-_k}\frac{\partial \boldsymbol{V}^-_k}{\partial t_{k-1}}\right)\delta t_{k-1}$$
$$+ \left(\frac{\partial \alpha_{kj}}{\partial \boldsymbol{R}_k} + \frac{\partial \alpha_{kj}}{\partial \boldsymbol{V}^+_k}\frac{\partial \boldsymbol{V}^+_k}{\partial \boldsymbol{R}_k} + \frac{\partial \alpha_{kj}}{\partial \boldsymbol{V}^-_k}\frac{\partial \boldsymbol{V}^-_k}{\partial \boldsymbol{R}_k}\right)\delta \boldsymbol{R}_k$$
$$+ \left(\frac{\partial \alpha_{kj}}{\partial t_k} + \frac{\partial \alpha_{kj}}{\partial \boldsymbol{V}^+_k}\frac{\partial \boldsymbol{V}^+_k}{\partial t_k} + \frac{\partial \alpha_{kj}}{\partial \boldsymbol{V}^-_k}\frac{\partial \boldsymbol{V}^-_k}{\partial t_k}\right)\delta t_k$$
$$+ \left(\frac{\partial \alpha_{kj}}{\partial \boldsymbol{V}^+_k}\frac{\partial \boldsymbol{V}^+_k}{\partial \boldsymbol{R}_{k+1}}\right)\delta \boldsymbol{R}_{k+1} + \left(\frac{\partial \alpha_{kj}}{\partial \boldsymbol{V}^+_k}\frac{\partial \boldsymbol{V}^+_k}{\partial t_{k+1}}\right)\delta t_{k+1} \tag{42}$$

The partial derivatives of $\boldsymbol{V}^+_k$ and $\boldsymbol{V}^-_k$ were previously identified and are summarized in Table 3. The only partials that remain to be evaluated are

$$\frac{\partial \alpha_{kj}}{\partial \boldsymbol{R}_k}, \qquad \frac{\partial \alpha_{kj}}{\partial t_k}, \qquad \frac{\partial \alpha_{kj}}{\partial \boldsymbol{V}^+_k}, \qquad \frac{\partial \alpha_{kj}}{\partial \boldsymbol{V}^-_k} \tag{43}$$

These partials will depend on the formulation of the constraint. Several examples are presented in the following sections. Functionally, the constraints are additional targets in the terminology used to describe the differential corrector. These are incorporated into the numerical process by augmenting the SRM matrix by one row for each scalar constraint. For instance, let $\boldsymbol{u} = [\delta \boldsymbol{R}_{k-1}, \delta t_{k-1}, \delta \boldsymbol{R}_k, \delta t_k, \delta \boldsymbol{R}_{k+1}, \delta t_{k+1}]^T$ represent the control vector associated with the kth patch point; then, $\boldsymbol{\alpha}_k$ is applied at this node such that $\boldsymbol{\alpha}_k = [\alpha_{k1}, \alpha_{k2}, \ldots, \alpha_{kj}]$. The level 2 corrector can yield a minimum-norm solution to the following linear system

$$\begin{bmatrix} \delta \Delta \boldsymbol{V}_k \\ \delta \boldsymbol{\alpha}_k \end{bmatrix} = \underbrace{\begin{bmatrix} \frac{\partial \Delta \boldsymbol{V}_k}{\partial \boldsymbol{u}} \\ \frac{\partial \boldsymbol{\alpha}}{\partial \boldsymbol{u}} \end{bmatrix}}_{\tilde{M}} \boldsymbol{u} \tag{44}$$

where $\boldsymbol{u} \in \mathbb{R}^{12\times 1}$ and $\tilde{M} \in \mathbb{R}^{(j+3)\times 12}$ is the augmented SRM matrix associated with the kth node. The following section summarizes the partial derivatives that are formulated to enforce a sample set of the more common constraints.

Sample Constraints: Partial Derivatives

In the following sections, the development of several sample constraints is presented. The general process of developing a constraint equation, and its associated partial derivatives, is independent of the dynamic regime. As long as the nonlinear system possesses a linear representation that can be expressed in terms of a state transition matrix, the two-level procedure is applicable. Basically, the fundamental algorithm seeks a solution that is continuous, smooth, and satisfies the nonlinear differential equations in the absence of constraints.

The periodicity constraint will, naturally, only be applicable to regimes where periodicity is possible. However, in this development, "periodicity" is not specific to the gravitational n-body problem. The partials are applicable to *any* dynamic system that exhibits periodic motion, even outside the field of astronautics. The two-level corrector, augmented by this constraint, simply seeks a solution to the nonlinear equations that is continuous, smooth, and periodic.

The velocity magnitude constraint allows for a nonsmooth solution. That is, the designer is able to specify a tolerance on the discontinuity between segments. For space applications, this type of design allowance is typically associated with nonzero impulsive maneuvers.

The flight-path angle, right ascension, and declination constraints, in this study, are applied to trajectory design in the n-body problem, which encompasses the two- and three-body problems as well. Ultimately, these constraints are designed to allow more control over the final geometry of the converged arc.

The specific energy constraint is unique to the two-body problem. Even in n-body analysis, this formulation of energy is often a prespecified design parameter, particularly for launch and return constraints. However, in the immediate vicinity of the planet, the two-body specific energy is an acceptable design parameter.

The final constraint considered here pertains to constraints with arbitrary centers. This constraint is not specific to any dynamic regime. In fact, this formulation addresses the issue of constraints that may be mathematically formulated in a different reference frame, with a different origin. No specific assumption concerning the dynamic regime is introduced.

Periodicity Constraint

In any corrections process, a startup solution is required. However, the startup arc does not necessarily have to satisfy all the constraints imposed on the trajectory. For instance, in the circular restricted three-body problem (CR3BP), the Richardson [14] series expansion offers an approximation to a three-dimensional periodic halo orbit that exists in the vicinity of a collinear libration point. Of course, if the results from this approximation are numerically integrated in the nonlinear CR3BP, the resulting arc is not periodic because the startup solution is only an initial guess.

Traditionally, a truly periodic halo orbit is identified by defining the initial state on the x axis and employing a simple differential corrector that targets a state on the first return to the x axis representing a half period ($T/2$) such that

$$\dot{x}_{T/2} = \dot{y}_{T/2} = y_{T/2} = 0 \tag{45}$$

This type of corrections approach exploits the known symmetry of the solution across the x–z plane in the rotating frame, where the trajectory achieves a perpendicular crossing at the point of maximum and minimum out-of-plane excursions. Of course, not all periodic

solutions in the CR3BP are symmetric across an easily identified plane. For example, the plane of symmetry is not necessarily obvious for orbits near L_4 and L_5. Also, for spacecraft formations near the libration points, periodic configurations are known to exist, but they are not necessarily symmetric. A standardized process is also sought to identify asymmetric periodic arcs, a goal achieved through the current methodology.

In essence, an asymmetric corrector is a generalized algorithm based on the standard two-level differential corrector originally developed by Howell and Pernicka [17]. Aside from state constraints, an extended corrector, developed by Wilson et al. [9,10,18,19], also allows for the inclusion of some algebraic constraints. The initial development of this process was successfully applied to the design of the Genesis trajectory [18,19]. The work presented here further extends this approach into a more general framework.

The search for asymmetric periodic arcs is initiated by imposing the following vector boundary constraint:

$$\boldsymbol{\alpha}_k = \boldsymbol{X}(t_1)^+ - \boldsymbol{X}(t_N)^- = \begin{bmatrix} \boldsymbol{R}_1 - \boldsymbol{R}_N \\ \boldsymbol{V}_1^+ - \boldsymbol{V}_N^- \end{bmatrix} \tag{46}$$

In this case, the startup solution is assumed to consist of N patch states; thus, $\boldsymbol{X}(t_1)^+$ is the initial state associated with the first segment along the trajectory, whereas $\boldsymbol{X}(t_N)^-$ represents the terminal state along the $N-1$ segment. Though the startup solution is not periodic, it is assumed that it is reasonably close to a periodic solution to provide an initial guess to the corrections process that is sufficient for convergence of the process. Note that $\boldsymbol{\alpha}_{k_j}$ is explicitly dependent on the position and velocity vectors associated with the initial and terminal points along the trajectory $\boldsymbol{\alpha}_k = \boldsymbol{\alpha}_k(\boldsymbol{R}_1, \boldsymbol{V}_1^+, \boldsymbol{R}_N, \boldsymbol{V}_N^-)$ and, through the velocity vectors, implicitly dependent on the time associated with these nodes. However, the constraint vector is also implicitly dependent on the positions and times associated with the node immediately after the first and the node just before the last:

$$\boldsymbol{V}_1^+ = \boldsymbol{V}_1^+(\boldsymbol{R}_1, t_1, \boldsymbol{R}_2, t_2) \tag{47}$$

$$\boldsymbol{V}_N^- = \boldsymbol{V}_N^-(\boldsymbol{R}_{N-1}, t_{N-1}, \boldsymbol{R}_N, t_N) \tag{48}$$

Thus, a Taylor series approximation of $\boldsymbol{\alpha}_k$, truncated to the first order, may be written

$$\begin{aligned}
\boldsymbol{\alpha}_k^* - \boldsymbol{\alpha}_k = {} & \left\{\frac{\partial \boldsymbol{\alpha}_k}{\partial \boldsymbol{R}_1} + \frac{\partial \boldsymbol{\alpha}_k}{\partial \boldsymbol{V}_1^+}\frac{\partial \boldsymbol{V}_1^+}{\partial \boldsymbol{R}_1}\right\}\delta\boldsymbol{R}_1 + \left\{\frac{\partial \boldsymbol{\alpha}_k}{\partial t_1} + \frac{\partial \boldsymbol{\alpha}_k}{\partial \boldsymbol{V}_1^+}\frac{\partial \boldsymbol{V}_1^+}{\partial t_1}\right\}\delta t_1 \\
& + \left\{\frac{\partial \boldsymbol{\alpha}_k}{\partial \boldsymbol{V}_1^+}\frac{\partial \boldsymbol{V}_1^+}{\partial \boldsymbol{R}_2}\right\}\delta\boldsymbol{R}_2 + \left\{\frac{\partial \boldsymbol{\alpha}_k}{\partial \boldsymbol{V}_1^+}\frac{\partial \boldsymbol{V}_1^+}{\partial t_2}\right\}\delta t_2 \\
& + \left\{\frac{\partial \boldsymbol{\alpha}_k}{\partial \boldsymbol{V}_N^-}\frac{\partial \boldsymbol{V}_N^-}{\partial \boldsymbol{R}_{N-1}}\right\}\delta\boldsymbol{R}_{N-1} + \left\{\frac{\partial \boldsymbol{\alpha}_k}{\partial \boldsymbol{V}_N^-}\frac{\partial \boldsymbol{V}_N^-}{\partial t_{N-1}}\right\}\delta t_{N-1} \\
& + \left\{\frac{\partial \boldsymbol{\alpha}_k}{\partial \boldsymbol{R}_N} + \frac{\partial \boldsymbol{\alpha}_k}{\partial \boldsymbol{V}_N^-}\frac{\partial \boldsymbol{V}_N^-}{\partial \boldsymbol{R}_N}\right\}\delta\boldsymbol{R}_N + \left\{\frac{\partial \boldsymbol{\alpha}_k}{\partial t_N} + \frac{\partial \boldsymbol{\alpha}_k}{\partial \boldsymbol{V}_N^-}\frac{\partial \boldsymbol{V}_N^-}{\partial t_N}\right\}\delta t_N
\end{aligned} \tag{49}$$

where $\boldsymbol{\alpha}_k^*$ represents the desired value of the constraint vector, in this case zero, to enforce periodicity. The partials with respect to $\boldsymbol{R}_1$, $\boldsymbol{V}_1^+$, $\boldsymbol{R}_N$, and $\boldsymbol{V}_N^-$ are straightforward and summarized as

$$\frac{\partial \boldsymbol{\alpha}_k}{\partial \boldsymbol{R}_1} = \begin{bmatrix} I \\ 0 \end{bmatrix} = -\frac{\partial \boldsymbol{\alpha}_k}{\partial \boldsymbol{R}_N} \tag{50}$$

$$\frac{\partial \boldsymbol{\alpha}_k}{\partial \boldsymbol{V}_1^+} = \begin{bmatrix} 0 \\ I \end{bmatrix} = -\frac{\partial \boldsymbol{\alpha}_k}{\partial \boldsymbol{V}_N^-} \tag{51}$$

The partials of $\boldsymbol{V}_N^-$ and $\boldsymbol{V}_1^+$, with respect to $\boldsymbol{R}_1, t_1, \boldsymbol{R}_2, t_2, \boldsymbol{R}_{N-1}, t_{N-1}$, $\boldsymbol{R}_N$, and t_N may subsequently be deduced from Table 1. The resulting approximation reveals that

$$\begin{aligned}
\boldsymbol{\alpha}_k^* - \boldsymbol{\alpha}_k = {} & \begin{bmatrix} I \\ -B_{21}^{-1}A_{21} \end{bmatrix}\delta\boldsymbol{R}_1 + \begin{bmatrix} 0 \\ \boldsymbol{a}_1^+ - D_{12}B_{12}^{-1}\boldsymbol{V}_1^+ \end{bmatrix}\delta t_1 \\
& + \begin{bmatrix} 0 \\ B_{21}^{-1} \end{bmatrix}\delta\boldsymbol{R}_2 + \begin{bmatrix} 0 \\ -B_{21}^{-1}\boldsymbol{V}_2^- \end{bmatrix}\delta t_2 + \left\{\begin{bmatrix} 0 \\ -B_{N-1,N}^{-1} \end{bmatrix}\right\}\delta\boldsymbol{R}_{N-1} \\
& + \left\{\begin{bmatrix} 0 \\ B_{N-1,N}^{-1}\boldsymbol{V}_N^+ \end{bmatrix}\right\}\delta t_{N-1} + \begin{bmatrix} -I \\ B_{N-1,N}^{-1}A_{N-1,N} \end{bmatrix}\delta\boldsymbol{R}_N \\
& + \left\{\begin{bmatrix} 0 \\ -(\boldsymbol{a}_N^- - D_{N,N-1}B_{N,N-1}^{-1}\boldsymbol{V}_N^-) \end{bmatrix}\right\}\delta t_N
\end{aligned} \tag{52}$$

Thus, given a set of N patch states that represents a nearly periodic startup solution, a standard two-level corrector, such as that in Eq. (32), can be augmented by Eq. (52) to identify any asymmetric periodic arc. In this study, this type of asymmetric corrections process is applied to identify periodic orbits near the L_4 and L_5 libration points, as well as asymmetric periodic arcs that are relative to a chief vehicle for formation flight.

Velocity Magnitude Constraint

If, instead of constraining the velocity vector directly, the magnitude of the velocity discontinuity is constrained, then the form of the constraint is

$$\alpha_{kj} = \left|\boldsymbol{V}_k^+ - \boldsymbol{V}_k^-\right| = \sqrt{\left(\boldsymbol{V}_k^+ - \boldsymbol{V}_k^-\right)\cdot\left(\boldsymbol{V}_k^+ - \boldsymbol{V}_k^-\right)} \tag{53}$$

The constraint is not an explicit function of position or time. Thus, the only nonzero partials are with respect to velocity:

$$\frac{\partial \alpha_{kj}}{\partial \boldsymbol{V}_k^+} = \frac{\left(\boldsymbol{V}_k^+ - \boldsymbol{V}_k^-\right)^T}{\left|\boldsymbol{V}_k^+ - \boldsymbol{V}_k^-\right|} \tag{54}$$

$$\frac{\partial \alpha_{kj}}{\partial \boldsymbol{V}_k^-} = -\frac{\left(\boldsymbol{V}_k^+ - \boldsymbol{V}_k^-\right)^T}{\left|\boldsymbol{V}_k^+ - \boldsymbol{V}_k^-\right|} \tag{55}$$

Note that these are essentially unit vectors in the direction of the current velocity discontinuity; the sign is plus or minus ensuring that it is parallel in either a positive or negative sense.

Flight-Path Angle Constraint

A constraint that is related to the apse condition is the constraint associated with the flight-path angle. Let the flight path angle γ be defined by the expression

$$\sin\gamma = \frac{\boldsymbol{R}_k \cdot \boldsymbol{V}_k}{|\boldsymbol{R}_k||\boldsymbol{V}_k|} \tag{56}$$

where $\boldsymbol{V}_k = \boldsymbol{V}_k^+$. For simplicity, and to avoid quadrant ambiguities, the constraint equation is formulated as

$$\alpha_{kj} = \sin\gamma - \sin\gamma_{\text{des}} \tag{57}$$

Then, the only nonzero constraint partials for the flight-path angle are

$$\frac{\partial \alpha_{kj}}{\partial \boldsymbol{R}_k} = \frac{\boldsymbol{V}_k^T}{|\boldsymbol{R}_k||\boldsymbol{V}_k|} - \frac{\boldsymbol{R}_k \cdot \boldsymbol{V}_k}{|\boldsymbol{R}_k|^2|\boldsymbol{V}_k|}\frac{\boldsymbol{R}_k^T}{|\boldsymbol{R}_k|} = \frac{\boldsymbol{V}_k^T}{|\boldsymbol{R}_k||\boldsymbol{V}_k|} - \sin\gamma\frac{\boldsymbol{R}_k^T}{|\boldsymbol{R}_k|^2} \tag{58}$$

$$\frac{\partial \alpha_{kj}}{\partial \boldsymbol{V}_k} = \frac{\boldsymbol{R}_k^T}{|\boldsymbol{R}_k||\boldsymbol{V}_k|} - \frac{\boldsymbol{R}_k \cdot \boldsymbol{V}_k}{|\boldsymbol{R}_k||\boldsymbol{V}_k|^2}\frac{\boldsymbol{V}_k^T}{|\boldsymbol{V}_k|} = \frac{\boldsymbol{R}_k^T}{|\boldsymbol{R}_k||\boldsymbol{V}_k|} - \sin\gamma\frac{\boldsymbol{V}_k^T}{|\boldsymbol{V}_k|^2} \tag{59}$$

Note that either the apse constraint or the flight-path angle constraint can be used to indirectly target true anomaly because true anomaly is related to both of these conditions.

Declination and Right Ascension Constraints

At a specific patch point, the orientation of $\boldsymbol{R}_k$ can be expressed in terms of right ascension ϕ and declination θ relative to some frame of reference. Let the reference frame be defined by unit vectors $\hat{x}$, $\hat{y}$, and $\hat{z}$ such that the declination and right ascension are evaluated as

$$\sin\theta = \frac{\boldsymbol{R}_k \cdot \hat{z}}{|\boldsymbol{R}_k|} \tag{60}$$

$$\tan\phi = \left(\frac{\boldsymbol{R}_k \cdot \hat{y}}{\boldsymbol{R}_k \cdot \hat{x}}\right) \tag{61}$$

The declination constraint may be stated as

$$\alpha_{kj} = \sin\theta - \sin\theta_{\text{des}} \tag{62}$$

In this case, the only nonzero constraint partial is

$$\frac{\partial \alpha_{kj}}{\partial \boldsymbol{R}_k} = \frac{1}{|\boldsymbol{R}_k|}\left[\hat{z}^T - \frac{\boldsymbol{R}_k^T}{|\boldsymbol{R}_k|}\sin\theta\right] \tag{63}$$

Similarly, the right ascension constraint may be represented as

$$\alpha_{kj} = \phi - \phi_{\text{des}} \tag{64}$$

Clearly, the partial relative to velocity is zero, whereas the partial relative to the position vector is

$$\begin{aligned}\frac{\partial \alpha_{kj}}{\partial \boldsymbol{R}_k} &= \left[1 + \left(\frac{\boldsymbol{R}_k \cdot \hat{y}}{\boldsymbol{R}_k \cdot \hat{x}}\right)^2\right]^{-1} \frac{\partial}{\partial \boldsymbol{R}_k}\left(\frac{\boldsymbol{R}_k \cdot \hat{y}}{\boldsymbol{R}_k \cdot \hat{x}}\right) \\ &= \frac{(\boldsymbol{R}_k \cdot \hat{x})\hat{y}^T - (\boldsymbol{R}_k \cdot \hat{y})\hat{x}^T}{(\boldsymbol{R}_k \cdot \hat{x})^2 + (\boldsymbol{R}_k \cdot \hat{y})^2}\end{aligned} \tag{65}$$

Right ascension is often evaluated relative to a frame that rotates with respect to the inertial frame, for example, the frame fixed to the rotating Earth. In this case, the constraint also possesses a time dependency. If the rotation rate of the frame ω relative to the inertial frame is assumed constant and ω is defined in the $\hat{z}$ direction, then the time derivative of the $\hat{x}$ and $\hat{y}$ unit vectors can be written in the form

$$\frac{\partial \hat{x}}{\partial t_k} = \omega\hat{y}, \qquad \frac{\partial \hat{y}}{\partial t_k} = -\omega\hat{x} \tag{66}$$

so that, ultimately, the constraint partial with respect to time reduces to

$$\frac{\partial \alpha_{kj}}{\partial t_k} = \omega \tag{67}$$

Specific Energy

Consider a constraint on the conic energy relative to an attracting body. Such a constraint can be written

$$\alpha_{kj} = \frac{1}{2}\boldsymbol{V}_k \cdot \boldsymbol{V}_k - \frac{\mu_p}{|\boldsymbol{R}_k|} = \frac{1}{2}\boldsymbol{V}_k \cdot \boldsymbol{V}_k - \frac{\mu_p}{\sqrt{\boldsymbol{R}_k \cdot \boldsymbol{R}_k}} \tag{68}$$

where μ_p is the gravitational constant for the desired body. The only nonzero constraint partials, in this case, are

$$\frac{\partial \alpha_{kj}}{\partial \boldsymbol{R}_k} = \frac{\mu_p \boldsymbol{R}_k^T}{|\boldsymbol{R}_k|^3} \tag{69}$$

$$\frac{\partial \alpha_{kj}}{\partial \boldsymbol{V}_k} = \boldsymbol{V}_k^T \tag{70}$$

Constraints with Arbitrary Centers

Some constraints may be defined relative to a specific reference point. For example, the apse [10] constraint is relative to a desired central body (the Earth, for instance). The patch points that define the trajectory are also associated with a center. However, a constraint defined at a particular patch point need not have the same center as that patch point. A constraint α_{kj} can be defined relative to a center A, that is,

$$\alpha_{kj} = \alpha_{kj}(t_k, {}_A\boldsymbol{R}_k, {}_A\boldsymbol{V}_k) \tag{71}$$

where ${}_A\boldsymbol{R}_k$ is the position of the kth node with respect to center A and ${}_A\boldsymbol{V}_k$ is the velocity (i.e., time derivative) of ${}_A\boldsymbol{R}_k$. If the state at the kth patch point is defined relative to some other reference center B, then the required constraint partials are

$$\frac{\partial \alpha_{kj}}{\partial t_k}; \qquad \frac{\partial \alpha_{kj}}{\partial {}_B\boldsymbol{R}_k}; \qquad \frac{\partial \alpha_{kj}}{\partial {}_B\boldsymbol{V}_k} \tag{72}$$

where the relationship between the state at the kth node relative to centers A and B is

$${}_B\boldsymbol{R}_k = {}_B\boldsymbol{R}_A + {}_A\boldsymbol{R}_k \tag{73}$$

$${}_B\boldsymbol{V}_k = {}_B\boldsymbol{V}_A + {}_A\boldsymbol{V}_k \tag{74}$$

Evaluation of the necessary partials is accomplished in either of two ways: 1) evaluate the constraint partials relative to A and then translate the results to B, or 2) translate the constraint definition to B and then evaluate the partials with respect to B. For example, if the apse constraint [10] is defined relative to center A as

$$\alpha_{kj} = {}_A\boldsymbol{R}_k \cdot {}_A\boldsymbol{V}_k \tag{75}$$

then the constraint partials with respect to center A are

$$\frac{\partial \alpha_{kj}}{\partial {}_A\boldsymbol{R}_k} = {}_A\boldsymbol{V}_k^T \tag{76}$$

$$\frac{\partial \alpha_{kj}}{\partial {}_A\boldsymbol{V}_k} = {}_A\boldsymbol{R}_k^T \tag{77}$$

Expressing these constraint partials relative to center B yields

$$\frac{\partial \alpha_{kj}}{\partial {}_B\boldsymbol{R}_k} = ({}_B\boldsymbol{V}_k - {}_A\boldsymbol{V}_B)^T \tag{78}$$

$$\frac{\partial \alpha_{kj}}{\partial {}_B\boldsymbol{V}_k} = ({}_B\boldsymbol{R}_k - {}_A\boldsymbol{R}_B)^T \tag{79}$$

If, however, α_{kj} is first expressed relative to center B, then

$$\alpha_{kj} = ({}_B\boldsymbol{R}_k - {}_A\boldsymbol{R}_B) \cdot ({}_A\boldsymbol{V}_k - {}_A\boldsymbol{V}_B) \tag{80}$$

so that

$$\frac{\partial \alpha_{kj}}{\partial {}_B\boldsymbol{R}_k} = ({}_B\boldsymbol{V}_k - {}_A\boldsymbol{V}_B)^T \tag{81}$$

$$\frac{\partial \alpha_{kj}}{\partial {}_B\boldsymbol{V}_k} = ({}_B\boldsymbol{R}_k - {}_A\boldsymbol{R}_B)^T \tag{82}$$

which is the same result that appears in Eqs. (78) and (79).

As an additional example, consider the nonlinear constraint related to velocity magnitude, i.e.,

$$\alpha_{kj} = {}_A\boldsymbol{V}_k \cdot {}_A\boldsymbol{V}_k \tag{83}$$

The constraint partials relative to center A are

$$\frac{\partial \alpha_{kj}}{\partial_A \boldsymbol{R}_k} = \boldsymbol{0}^T \tag{84}$$

$$\frac{\partial \alpha_{kj}}{\partial_A \boldsymbol{V}_k} = 2_A \boldsymbol{V}_k^T \tag{85}$$

Shifting the relationships in Eqs. (85) and (86) to center, B yields

$$\frac{\partial \alpha_{kj}}{\partial_B \boldsymbol{R}_k} = \boldsymbol{0}^T \tag{86}$$

$$\frac{\partial \alpha_{kj}}{\partial_B \boldsymbol{V}_k} = 2\left({}_A\boldsymbol{V}_k^T - {}_A\boldsymbol{V}_B^T\right) \tag{87}$$

Modifying the center of the constraint produces

$$\alpha_{kj} = ({}_B\boldsymbol{V}_k - {}_A\boldsymbol{V}_B)\cdot({}_B\boldsymbol{V}_k - {}_A\boldsymbol{V}_B) = {}_B\boldsymbol{V}_k \cdot {}_B\boldsymbol{V}_k - 2_A\boldsymbol{V}_B \cdot {}_B\boldsymbol{V}_k + {}_A\boldsymbol{V}_B \cdot {}_A\boldsymbol{V}_B \tag{88}$$

The constraint partials relative to center B are once again

$$\frac{\partial \alpha_{kj}}{\partial_B \boldsymbol{R}_k} = \boldsymbol{0}^T \tag{89}$$

$$\frac{\partial \alpha_{kj}}{\partial_B \boldsymbol{V}_k} = 2({}_B\boldsymbol{V}_k - {}_A\boldsymbol{V}_B)^T \tag{90}$$

the same result originally presented in Eq. (87).

Results

Example 1: Asymmetric Periodic Orbits Near L_4 and L_5

In the late 1970s, Markellos and Halioulias [20] briefly explored the identification of asymmetric periodic arcs in the general CR3BP. Later, Zagouras [21] and Papadakis [22] focus more specifically on the identification of periodic orbits near the triangular points of the CR3BP. In the late 1990s, Zagouras et al. [23] also identified some asymmetric orbits near the triangular points. Although the existence of symmetric and asymmetric periodic arcs in the CR3BP has been extensively studied, a subset of arcs near L_4 and L_5 is selected here to illustrate the success and robustness of the asymmetric corrections process. The advantage of this methodology, as previously stated, is that it requires no knowledge of the symmetry, or asymmetry, of the orbit. All that is necessary is an initial guess that is nearly periodic, regardless of the overall geometrical features.

Near the triangular points, in the CR3BP, one possible method for acquiring a startup periodic arc is the Floquet analysis presented by Howell and Marchand [13]. The analysis presented in [13] is originally intended to assist in the identification of bounded relative motions for formation flight applications. However, this same approach is easily adapted here to the identification of periodic orbits near L_4 and L_5. In this example, bounded or periodic motions are sought near L_4. To that end, consider the linear stability properties of this triangular point.

In the sun–Earth/moon system, evaluation of the Jacobian matrix, in Eq. (4), reveals that the L_4 libration point has six neutrally stable eigenvalues,

$$\lambda_{1,2} = \pm j.99999, \qquad \lambda_{3,4} = \pm j.0045353, \qquad \lambda_{5,6} = \pm j \tag{91}$$

and six linearly independent eigenvectors. These eigenvectors, or modes, are indicative of the existence of three different types of motion near the L_4 libration point. A sample set of solutions, obtained by exciting modes 1–2, 3–4, or 5–6, are illustrated in Figs. 4 and 5.

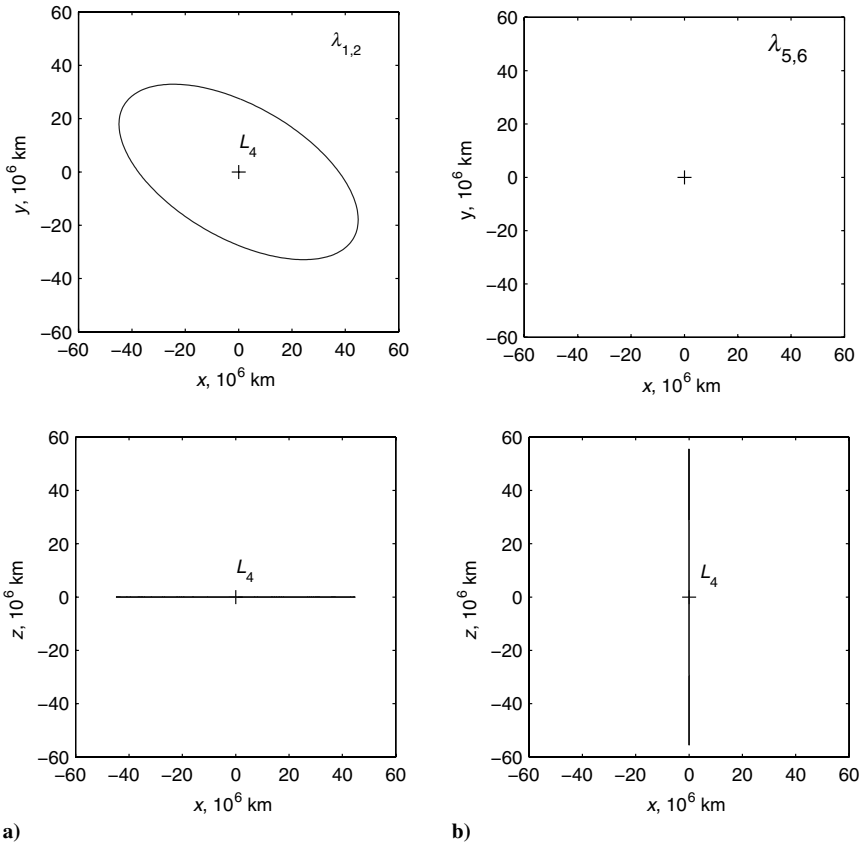

Fig. 4 Linearized short-period natural motions near L_4.

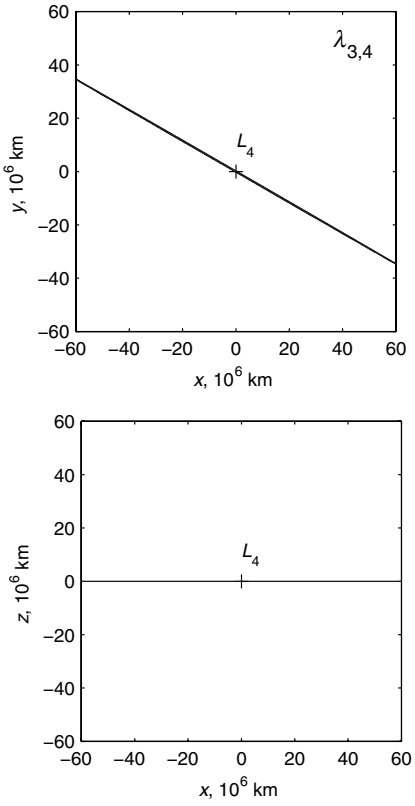

Fig. 5 Linearized long-period natural motion near L_4.

The $\lambda_{3,4}$ eigenvalues are associated with the long-period mode, roughly 221 years, and correspond to the sample solution in Fig. 5. The remaining eigenvalues are associated with short-period modes of about 1 year each, and the sample orbits are those illustrated in Fig. 4. In the present investigation, only the short-period modes are of interest. To illustrate the effectiveness of the asymmetric corrections process, consider the sample rectilinear vertical orbit in Fig. 4b. A sample set of patch states along this rectilinear path are selected as a startup solution to the corrections process described earlier. Again, note that this corrector makes no assumptions about the shape or symmetry properties of the orbit. Thus, the patch point selection is somewhat arbitrary, though selecting a set of states that is representative of the orbit geometry can enhance the convergence properties of the algorithm. In the nonlinear system, the corrections process is able to numerically establish a nearly vertical orbit, though not rectilinear, that closely resembles that in Fig. 4b. The results of this process, using the curve in Fig. 4b as a startup arc, appear in Fig. 6.

The two short-period modes may also be combined to generate generally three-dimensional orbits. However, to ensure that the geometry of the startup arc is preserved during the corrections process, additional interior constraints may be necessary. To better illustrate this, consider the sample startup solution in Fig. 7.

From the solution in Fig. 7, five patch points are selected for the differential corrections process, as depicted in Fig. 8. The initial and terminal patch states are arbitrarily selected along the orbit and are labeled as points one and five. To preserve the overall features of this orbit during the corrections process, control points are strategically introduced at the second and fourth patch states, where the orbit achieves extremal values in the z component. For instance, let $z_{k\text{des}}$ represent the desired value of the z component at the kth patch state, for $k = 2$.

In addition to the periodicity constraint, implemented at patch states one and five, the corrector matrix is also augmented to incorporate the following constraints [24]:

$$\boldsymbol{\alpha}_2 = \begin{bmatrix} z_2 - z_{2_{\text{des}}} \\ \dot{z}_2^+ \end{bmatrix} \tag{92}$$

The nonzero constraint partials, associated with Eq. (92), are defined as

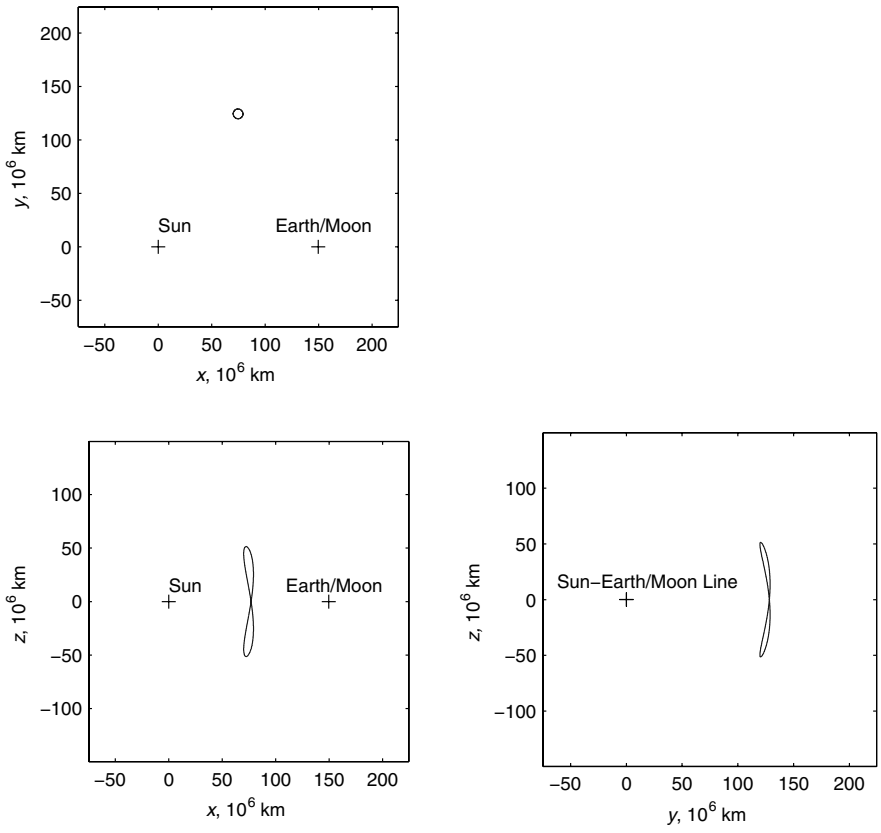

Fig. 6 Converged vertical orbit near L_4, determined in the nonlinear CR3BP.

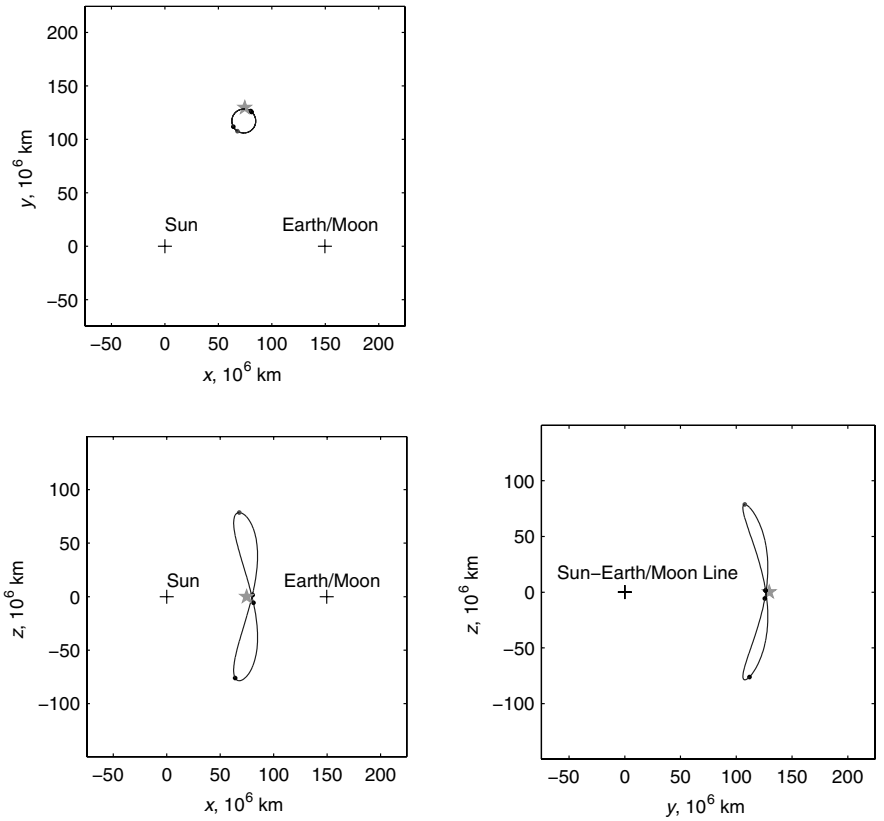

Fig. 7 Sample sun–Earth/moon L_4 orbit obtained via Floquet analysis and asymmetric corrector.

$$\frac{\partial \boldsymbol{\alpha}_2}{\partial \boldsymbol{R}_2} = \begin{bmatrix} 0 & 0 & 1 \\ 0 & 0 & 0 \end{bmatrix} \tag{93}$$

$$\frac{\partial \boldsymbol{\alpha}_2}{\partial \boldsymbol{V}_2^+} = \begin{bmatrix} 0 & 0 & 0 \\ 0 & 0 & 1 \end{bmatrix} \tag{94}$$

Alternatively, if the initial startup arc already exhibits the desired z_2, one may simply fix the variation on this coordinate and augment the SRM using only the velocity constraint in Eq. (92). The preceding results are substituted into Eq. (42) and the resulting variational equation augments the SRM for the corrections process. Once a solution is reestablished in the nonlinear system, the resulting trajectory may be used as a startup arc in generating the L_4 vertical orbit family. This step is easily accomplished via a simple numerical continuation process. For example, in Fig. 8, $z_{2\text{des}}$ may be increased with every successful completion of the corrector to generate the family in Fig. 9.

When the vertical L_4 family in Fig. 9 reaches a critical amplitude, i.e., a bifurcation, additional constraints are necessary to ensure the continuation remains within the vertical family. Similarly, an alternate set of constraints may be established to follow along the axial family of orbits. Specifically, x_2 is constrained to some specified target values $x_{2\text{des}}$, whereas z_2 is free. The results of such propagation are illustrated in Fig. 10.

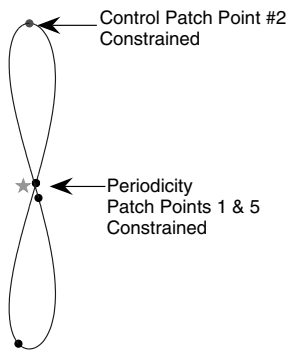

Fig. 8 Location of patch states along startup solution and details of state constraints at each patch point.

In the nonlinear model, this methodology is successfully adapted to the identification of periodic orbits near any of the collinear points, or relative periodic paths in the formation flight problem [13]. Of course, this methodology is not restricted to the identification of periodic orbits. For example, the constraint formulations involving the radial distance, apse condition, time, and inclination [10] combined with the additional endpoint constraints presented here, were successfully employed in the design of the Genesis trajectory [18,19].

Example 2: Genesis Trajectory Design

In the initial Genesis design [18], originally scheduled for a February 2001 launch as illustrated in Fig. 11, the corrections process was divided into a launch phase, an orbit phase, and a return phase. However, the methodology presented here was also successfully applied to an end-to-end design [19], where the launch leg, the Lissajous trajectory, and the return leg were simultaneously corrected as a single continuous constrained trajectory in the ephemeris model. Interior nonzero maneuvers were necessary to meet all the mission constraints. To implement these maneuvers, the velocity discontinuity constraint at a specific patch point is relaxed by specifying a maximum allowable maneuver. The resulting trajectory, for an August–September 2001 launch window, is illustrated in Fig. 12. The surface in Fig. 12 represents a collection of solutions, generated at one day intervals, with radial, apse, and inclination constraints applied at the launch point, right ascension, declination, radial, and flight-path angle constraints applied at the terminal state, and interior constraints to restrict the magnitude of the maneuvers, including the Lissajous orbit insertion (LOI) maneuver.

Example 3: Periodic Formations near the Collinear Points

The asymmetric corrector employed in example 1 is successfully applied to the identification of relative periodic orbits, in the nonlinear model, for two spacecraft flying in formation near the L_1

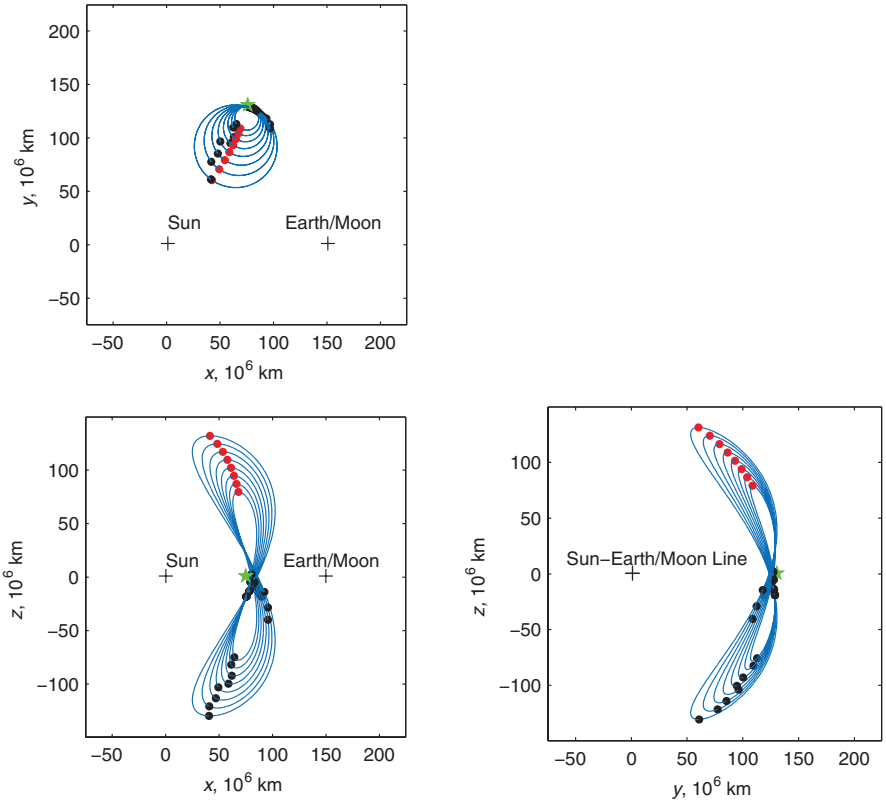

Fig. 9 Neighboring L_4 family of orbits obtained by varying the terminal z value in the asymmetric corrector.

and L_2 libration points. Howell and Marchand [13] identify a number of periodic and slowly drifting relative orbits for two spacecraft flying in formation in the vicinity of an L_1/L_2 halo orbit. The identification of the startup arcs is, once again, facilitated by a Floquet approach [13]. The process of transitioning these periodic arcs into the nonlinear model is accomplished through the use of the asymmetric corrector discussed here. Figure 13 illustrates an example where the initial arc is closed through the addition of nonzero impulsive maneuvers at two points along the trajectory. Within one or two iterations, the asymmetric corrector quickly

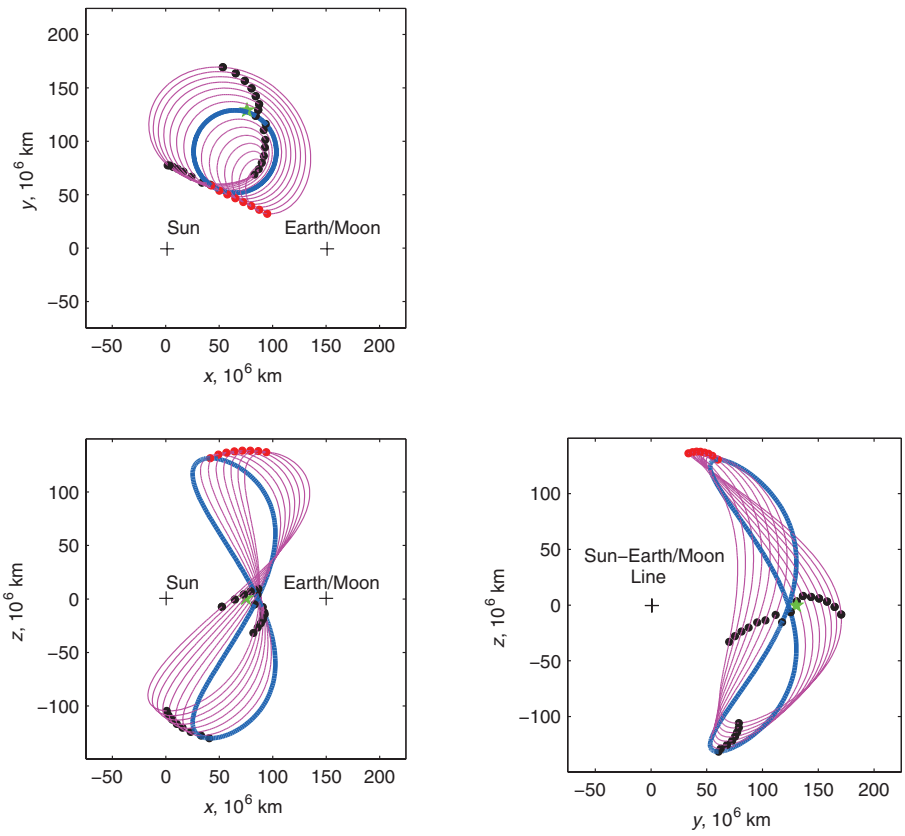

Fig. 10 Results of arbitrary L_4 family propagation along y axis.

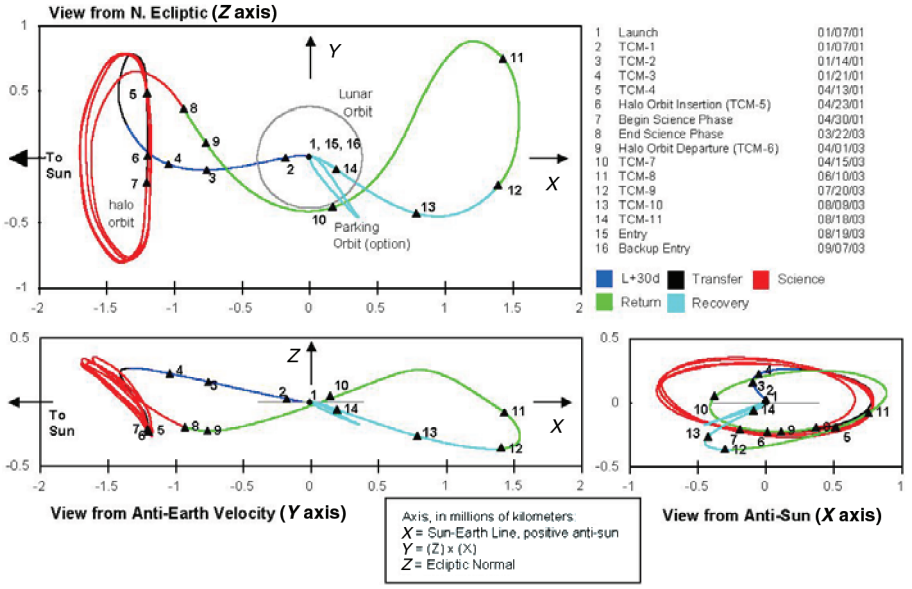

Fig. 11 Initial Genesis trajectory design (courtesy NASA/JPL-Caltech).

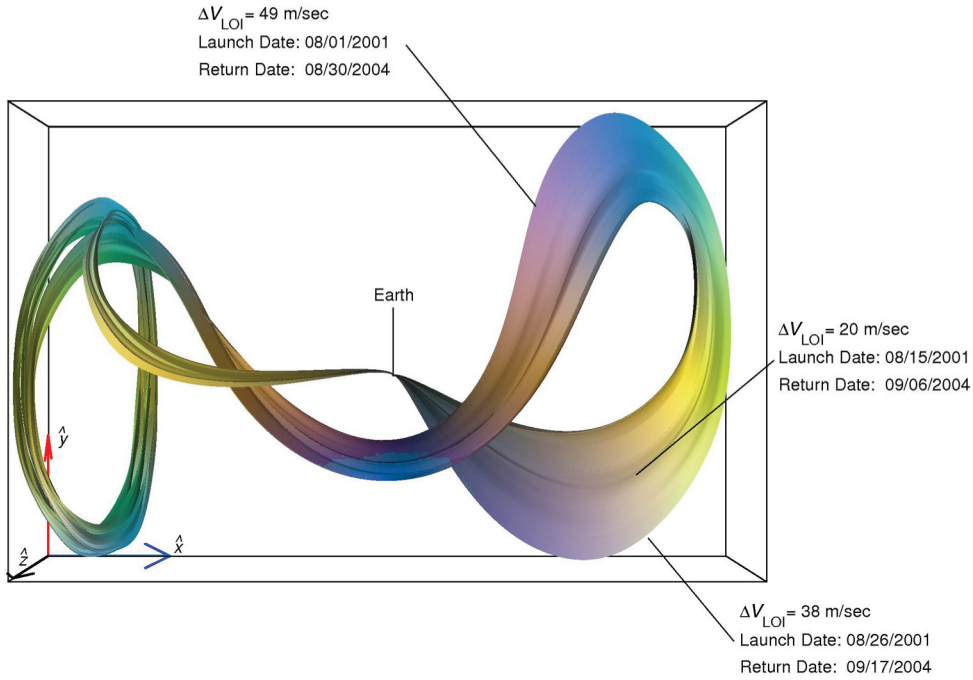

Fig. 12 Genesis summer 2001 launch options.

identifies the neighboring periodic arc and drives the initial maneuvers to zero.

Conclusions

In this investigation, an asymmetric constrained differential corrector is presented. An immediate advantage of this approach, particularly for the identification of periodic orbits, is that the startup arc need not exhibit any symmetry for the methodology to achieve the formulated objectives or satisfy the imposed interior and exterior constraints. The versatility and generality of the two-level constrained differential corrector is demonstrated through three distinct examples: the identification of asymmetric periodic orbits near the triangular points, the end-to-end constrained design of the Genesis trajectory, and the identification of periodic relative arcs in the formation flight problem.

For autonomous dynamic systems, the methodology is successfully applied to the identification of trajectory arcs subject to algebraic constraints, periodic orbits, quasi-periodic trajectories, or combinations thereof. It is important to note that the process is in no way exclusive to the gravitational n-body problem or spacecraft mission design. If the dynamic system is autonomous, the constraints can be specified algebraically, and the constraint derivatives exist, the methodology is easily adapted to a variety of applications. For spacecraft mission design, however, the results of this investigation demonstrate that the asymmetric constrained differential corrector is able to minimize velocity discontinuities and enforce constraints in a cohesive manner, and proves to be an efficient end-to-end design tool.

Acknowledgments

The authors extend their appreciation to Daniel Grebow, from Purdue University, for his contributions to the implementation of example 1. Portions of this work were completed at Purdue University and the Jet Propulsion Laboratory, California Institute of Technology under contract with NASA.

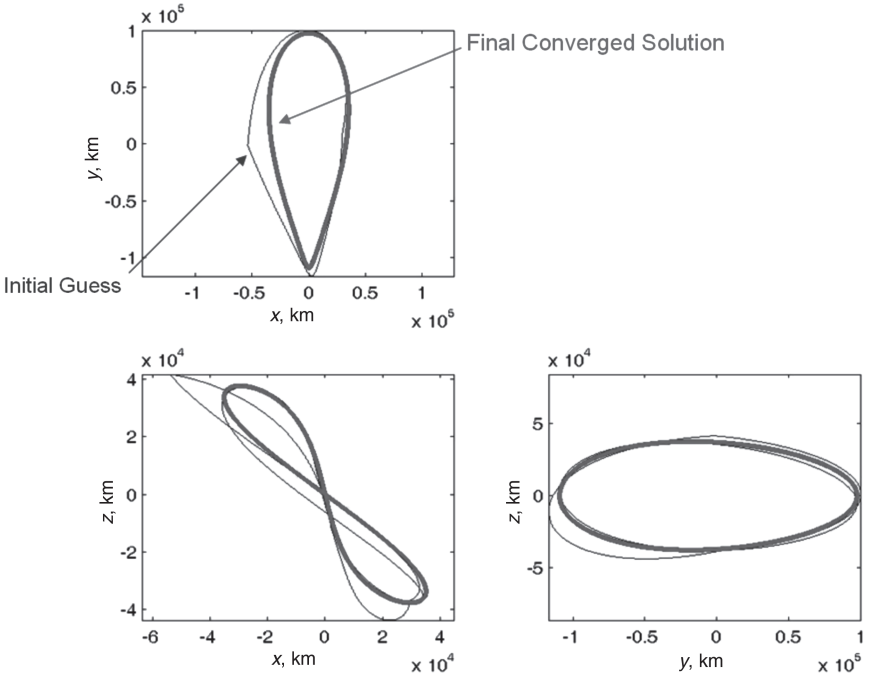

Fig. 13 Periodic relative path near a spacecraft evolving along an L_2 halo orbit.

References

[1] Poincaré, H., *New Methods of Celestial Mechanics*, Vol. 1, American Inst. of Physics, New York, 1993; also Periodic and Asymptotic Solutions, Translated from the French, Revised Reprint of the 1967 English Translation, with Endnotes by V. I. Arnold, Edited and with an Introduction by D. L. Goroff.

[2] Farquhar, R. W., Muhonen, D. P., Newman, C. R., and Heuberger, H. S., "Trajectories and Orbital Maneuvers for the First Libration-Point Satellite," *Journal of Guidance and Control*, Vol. 3, No. 6, 1980, pp. 549–554.

[3] Farquhar, R. W., "Flight of ISEE-3/ICE: Origins, Mission History, and a Legacy," *Journal of the Astronautical Sciences*, Vol. 49, No. 1, 2001, pp. 23–73.

[4] Dunham, D. W., Jen, S. J., Roberts, C. E., Seacord, A. W., II, Sharer, P. J., Folta, D. C., and Muhonen, D. P., "Double Lunar-Swingby Trajectories for the Spacecraft of the International Solar-Terrestrial Physics Program," *Orbital Mechanics and Mission Design: Advances in the Astronautical Sciences, AAS/NASA International Symposium*, Vol. 69, American Astronautical Society, 1989, pp. 285–301.

[5] Dunham, D. W., Jen, S. J., Roberts, C. E., Seacord, A. W., II, Sharer, P. J., Folta, D. C., and Muhonen, D. P., "Transfer Trajectory Design for the SOHO Libration-Point Mission," *43rd International Astronautical Congress, Washington*, International Astronautical Federation Paper 92-0066, 1992.

[6] Stone, E. C., Frandsen, A. M., Mewaldt, R. A., Christian, E. R., Margolies, D., Ormes, J. F., and Snow, F., "Advanced Composition Explorer," *Space Science Reviews*, Vol. 86, Nos. 1–4, 1998, pp. 1–22.

[7] Cuevas, O., Kraft-Newman, L., Mesearch, M., and Woodard, M., "Overview of Trajectory Design Operations for the Microwave Anisotropy Probe Mission," *AIAA/AAS Astrodynamics Specialist Conference and Exhibit*, AIAA Paper 2002-4425, 2002.

[8] Lo, M., Williams, B., Bollman, W., Han, D., Hahn, Y., Bell, J., Hirst, E., Corwin, R., Hong, P., Howell, K. C., Barden, B., and Wilson, R., "GENESIS Mission Design," *Journal of the Astronautical Sciences*, Vol. 49, No. 1, 2001, pp. 169–184.

[9] Wilson, R. S., "Trajectory Design in the Sun-Earth-Moon Four Body Problem," Ph.D. Dissertation, School of Aeronautics and Astronautics, Purdue Univ., West Lafayette, IN, 1998.

[10] Wilson, R. S., and Howell, K. C., "Trajectory Design in the Sun-Earth-Moon System Using Lunar Gravity Assists," *Journal of Spacecraft and Rockets*, Vol. 35, No. 2, 1998, pp. 191–198.

[11] Howell, K. C., "Three-Dimensional Periodic Halo Orbits," *Celestial Mechanics*, Vol. 32, No. 1, 1984, pp. 53–71.

[12] Markellos, V. V., "Three-Dimensional General Three-Body Problem: Determination of Periodic Orbits," *Celestial Mechanics*, Vol. 21, No. 3, 1980, pp. 291–309.

[13] Howell, K. C., and Marchand, B. G., "Natural and Non-Natural Spacecraft Formations Near the L1 and L2 Libration Points in the Sun-Earth/Moon Ephemeris System,," *Dynamical Systems: an International Journal*, Special Issue "Dynamical Systems in Dynamical Astronomy and Space Mission Design, Vol. 20, No. 1, 2005, pp. 149–173.

[14] Richardson, D. L., "Analytic Construction of Periodic Orbits About the Collinear Points," *Celestial Mechanics*, Vol. 22, No. 3, 1980, pp. 241–253.

[15] Richardson, D. L., and Cary, N. D., "Uniformly Valid Solution for Motion about the Interior Libration Point of the Perturbed Elliptic-Restricted Problem," *AAS/AIAA Astrodynamics Specialists Conference*, American Astronautical Society Paper 75-021, 1975.

[16] Howell, K. C., Marchand, B. G., and Lo, M. W., "Temporary Satellite Capture of Short-Period Jupiter Family Comets from the Perspective of Dynamical Systems," *Journal of the Astronautical Sciences*, Vol. 49, No. 4, 2001, pp. 539–557.

[17] Howell, K. C., and Pernicka, H. J., "Numerical Determination of Lissajous Trajectories in the Restricted Three-Body Problem," *Celestial Mechanics*, Vol. 41, Nos. 1–4, 1987, pp. 107–124.

[18] Howell, K. C., Barden, B. T., Wilson, R. S., and Lo, M. W., "Trajectory Design Using a Dynamical Systems Approach with Application to GENESIS," *AAS/AIAA Astrodynamics Conference, Sun Valley, Idaho*, American Astronautical Society Paper 97-7091997, pp. 1665–1684.

[19] Wilson, R. S., Barden, B. T., Howell, K. C., and Marchand, B. G., "Summer Launch Options for the Genesis Mission," *Advances in the Astronautical Sciences*, Vol. 109, Part 1, 2002, pp. 77–94.

[20] Markellos, V. V., and Halioulias, A. A., "Numerical Determination of Asymmetric Periodic Solutions," *Astrophysics and Space Science*, Vol. 46, No. 1, 1977, pp. 183–193.

[21] Zagouras, C. G., "Three Dimensional Periodic Orbits about the Triangular Equilibrium Points of the Restricted Problem of Three Bodies," *Celestial Mechanics*, Vol. 37, No. 1, 1985, pp. 27–46.

[22] Papadakis, K. E., and Zagouras, C. G., "Bifurcation Points and Intersections of Families of Periodic Orbits in the Three-Dimensional Restricted Three-Body Problem," *Astrophysics and Space Science*, Vol. 199, No. 2, 1993, pp. 241–256.

[23] Zagouras, C. G., Perdois, E., and Ragos, O., "New Kinds of Asymmetric Periodic Orbits in the Restricted Three-Body Problem," *Astrophysics and Space Science*, Vol. 240, No. 2, 1996, pp. 273–293.

[24] Grebow, D. J., "Generating Periodic Orbits in the Circular Restricted Three-body Problem with Applications to Lunar South Pole Coverage," M.S. Thesis, School of Aeronautics and Astronautics, Purdue Univ., West Lafayette, IN, 2006.

C. Kluever
Associate Editor